Observations of two young core-collapse supernova remnants

Observations of two young core-collapse supernova remnants

The Crab nebula and SN 1987A

Anestis Tziamtzis

Stockholm University

ISSN 1651-6214
ISBN 91-554-5436-4

Printed in Sweden by Intellecta Docusys, Stockholm 2011

Distributor: Department of Astronomy, Stockholm University

The earth, a purple blaze
Of saphire haze in orbital ways
While down below the trees
Bathed in cool breeze
Silver starlight breaks dawn from night
And so we pass on by
The crimson eye of great god Mars
As we travel the universe

Terence Michael Joseph Butler

Amongst others to Dimitri, Helen, and Christina

This thesis is based on the following four scientific articles, re-printed in the second part of the thesis. The articles present studies on the Crab nebula & SN 1987A.

I. Observational and theoretical constraints for an Hα-halo around the Crab nebula. Tziamtzis, A., Schirmer, M., Lundqvist, P., & Sollerman, J., 2009, A&A, 497, 167

II. The Crab pulsar and its pulsar-wind nebula in the optical and infrared. Tziamtzis, A., Lundqvist, P., & Djupvik, A. A., 2009, A&A, 508, 221

III. The outer rings of SN1987A. Tziamtzis, A., Lundqvist, P., Gröningsson, P. & Nasoudi-Shoar, S. 2010, A&A, 572, 35

IV. Constraints on fast ejecta in the Crab Nebula from optical spectral lines. Lundqvist P. & Tziamtzis A., 2011, submitted to A&A

Contents

Part I:
Introduction

1. Introduction

Supernova (SN) explosions are among the most energetic of events that take place in the Universe. They occur when stars end their lives. A star with $M \geq 9\ M_{\odot}$ will evolve until its core collapses under its own gravity, and it explodes as a core collapse supernova by blowing off its envelope (Heger et al. 2003). In this type of explosion a compact remnant can be left over, either in the form of a high density neutron star, or in more extreme cases, a black hole. Stars that are less massive follow a different path in their evolution and can form a carbon-oxygen white dwarf (Heger et al. 2003). In this case, in order for there to be an explosion, the white dwarf needs a companion star from where it accretes matter until it reaches an upper mass limit, known as the Chandrasekhar mass ($\sim$1.4 $M_{\odot}$) and then it explodes without leaving a compact remnant. This type of supernova is called Type Ia.

The energy that is released in a core-collapse supernova explosion is around 10^{53} ergs. Almost all of this energy ($\sim$99 %) is radiated away in the form of neutrinos which leaves a kinetic energy of around 10^{51} ergs. This energy, however, is still enough to eject matter at velocities of 10^{4} km s^{-1} (Schawinski et al. 2008). Apart from being spectacular events in the Universe, many pieces of information can be obtained from supernova explosions and the evolution of their remnants. For example, through supernova studies we can understand the late stages of stellar evolution, improve our knowledge of shock physics, particle acceleration (Vink 2004), triggered star formation (Preibisch & Zinnecker 2001) and nucleosynthesis. Stars are the objects that create heavy elements ($Z \geq 4$), and with their stellar winds and possible subsequent explosions all these elements are distributed in the Universe making life possible.

Supernovae can also be used for cosmology (Perlmutter et al. 1997) because they are excellent standard candles, especially Type Ia supernovae. They enable us estimate the expansion history of the Universe by examining the relationship between the distance from an object and its redshift, thus estimating how fast it is receding from us. Since Type Ia supernovae are considered to arise from thermonuclear explosions of carbon-oxygen white dwarfs (Leibundgut 2000), the uniformity of mass and similarity of chemical composition for Type Ia progenitors could explain why these supernovae are particularly good standard candles, or at least standardizable candles. This type of supernova is not covered by this thesis.

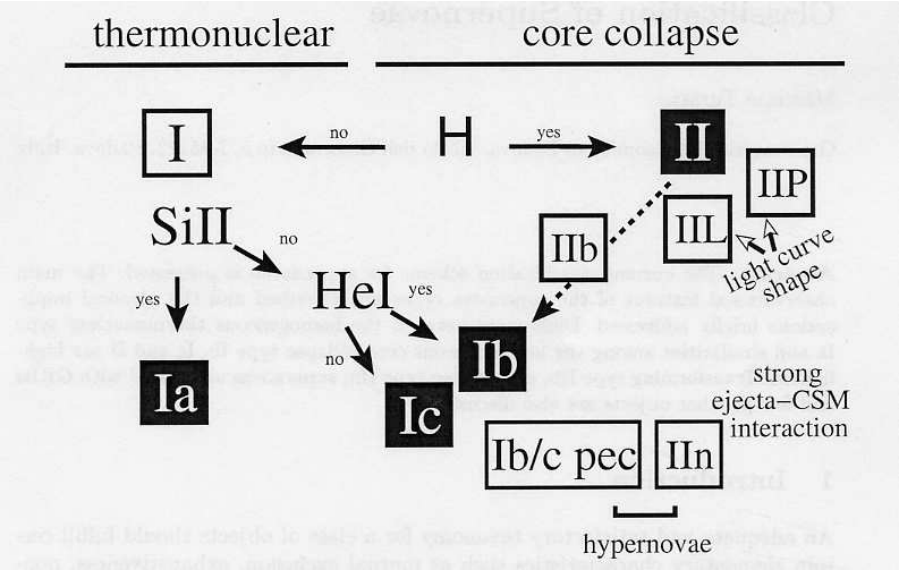

Figure 1.1: Classification of supernovae according to their spectral and photometric features. Only Type Ia SNe are associated with thermonuclear explosions, while the rest of them are associated with core-collapse of massive stars ($M \geq 9\ M_{\odot}$). Some Type Ib/c and IIn events with high explosion energies ($E \geq 10^{52}$ ergs) are usually referred to as hypernovae. At least some Type Ic supernovae are believed to be the sources of γ-ray bursts. (From Turatto 2003)

1.1 Classification of supernovae

The taxonomy of supernovae is based on their spectroscopic and photometric features. Originally, Minkowski (1941) introduced two distinct types of supernovae, based on the presence or not of hydrogen in their spectra. Thus Type I events are classified the supernovae that lack hydrogen lines in their spectra, while those that display hydrogen lines in their spectra as Type II. As telescopes and instrumentation improved it was realised that there are differences within the two classes of supernovae, thus new subclasses were introduced, to explain the spectroscopic and photometric properties of supernovae.

In the 80s it was realised that the strict division between Type I and Type II, based on the presence of hydrogen, or not, in the spectrum was not enough. This led to the introduction of new subclasses of supernovae. Thus supernovae that lack hydrogen and helium lines and which display a strong Si II absorption at 6150 Å are classified as Type Ia. For the supernovae that do not display hydrogen lines in the spectra, and for which the Si II absorption is absent, the Type Ib and Ic subclasses were introduced. The difference between Type Ib and Ic is that the spectra of Type Ib supernovae display helium lines (see Fig 1.1). Type Ia supernovae are observed in every type of galaxy (including ellipticals), and based on the fact that they lack the most abundant elements in

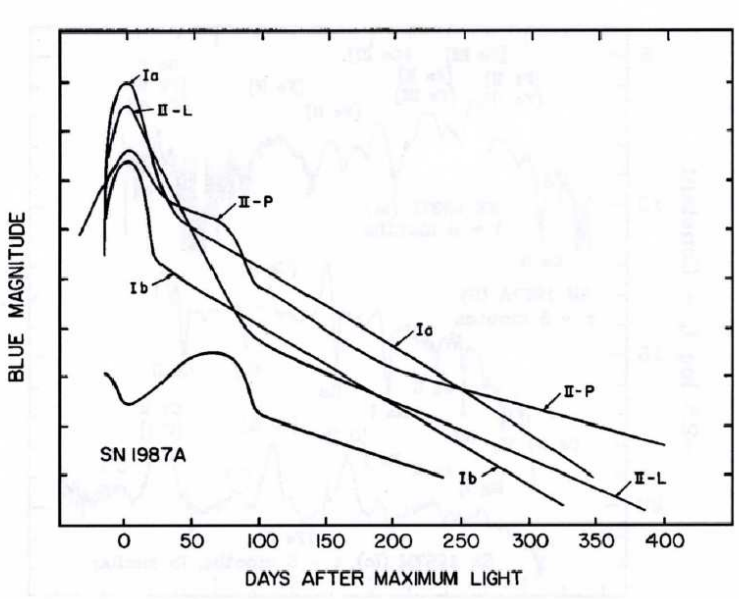

Figure 1.2: Schematic lightcurves of supernovae Type Ia, Ib, IIL IIP and SN 1987A. The lightcurve for SNe Ib includes also Type Ic as well and it represents an average (From Filippenko 1997).

the universe (H & He), it is believed that they are associated with explosion of white dwarfs. Type Ib/c supernovae, on the other hand, may also lack hydrogen lines, but they appear only in the spiral arms of galaxies, where star formation takes place. Thus it is believed that they are associated with the core-collapse of massive stars which have lost their hydrogen envelope (Type Ib), and in some cases also their helium envelope (Type Ic).

Type II supernovae are divided into four subclasses. The two major subclasses are Type IIP and Type IIL, which are distinguished from the difference in their respective light curves. Supernovae that are classified as Type IIP retain a massive hydrogen envelope at the moment of the explosion, thus after maximum light they display a plateau phase (see Fig 1.2) that lasts for a period of 3-4 months. During this period the supernova is powered by the recombination of its hydrogen envelope. Type IIL supernovae retain a smaller hydrogen envelope (≤ 2 $M_{\odot}$), thus their light curve decline is linear.

Some Type II supernovae are characterised by strong Balmer lines, and at early times they display blue continua spectra. These supernova seem to interact with their dense circumstellar medium (CSM). Their spectra are dominated by strong emission lines with very narrow profiles. These supernovae are classified as Type IIn, where the narrow and broad-base components of the line profiles stem from the ejecta interaction with the CSM in combination

with scattering of the line photons (Chugai et al. 2004 and Dessart et al. 2009 for models of SN 1994W).

Finally, there is another class of supernovae that seem to be an intermediate class between the Type II subclasses and the Type Ib/c supernovae. These supernovae are known as Type IIb with SN 1993J being the most famous case. These supernovae arise from massive stars which prior to the explosion have retained a thin hydrogen envelope. They initially display spectra with hydrogen lines like a Type IIL, but as their ejecta expand, their hydrogen lines become weaker, and then eventually their spectra switch to spectra similar to Type Ib.

1.2 Evolutionary effects

As mentioned above, core collapse supernovae show a diversity in terms of their spectroscopic and photometric properties. Responsible for this diversity are the various evolution paths that massive stars follow, due to their physical properties. These are the initial mass and metallicity, and below we discuss how such properties can affect the mass loss and evolution of a star, leading to the various types of supernova explosions. This section closes by discussing the evolution of massive stars, when these are part of a binary system. The discussion is based on the models from Heger et al. (2003) for the evolution of massive stars (≥ 9 $M_{\odot}$).

1.2.1 Nature of the winds

A stellar wind is described as the outflow of charged or neutral gas from the atmosphere of a star. The nature of the wind for an isolated star, depends on the type of the star (i.e., red or blue giant), the metallicity and the initial mass. The wind intensity is very important for the evolution of the star, since it influences the star's size, luminosity, and surface temperature, as well as the type of the supernova explosion.

Blue supergiants (BSG) have winds with a mass loss rate $\dot{M} \leq 10^{-5}$ $M_{\odot}$ yr^{-1}, and they can lose up to 50% of their mass while on the main sequence. The nature of these winds is well understood and they are mainly due to resonance line scattering of UV radiation. A characteristic of such a wind is that its velocity is roughly equal to the escape velocity, thus the velocity ranges from $\sim$ 1000 - 3000 km s^{-1}.

Stars in their red supergiant (RSG) phase also display winds where their mass loss rate is $\sim \dot{M} \leq 10^{-6}$ $M_{\odot}$ yr^{-1}, while on their super-wind phase, the mass loss can be as high as $\sim \dot{M} \sim 10^{-3} - 10^{-4}$ $M_{\odot}$ yr^{-1}. These kinds of

winds are not as well understood as those of BSG, but it is believed that they are due to absorption of radiation by dust. This is probably the case for stars with smaller masses (< 8 $M_\odot$) that evolve as AGB stars, and then to white dwarfs. Since a RSG is more extended than a BSG, its escape velocity is in the order $\sim$ 10 - 20 km s^{-1}.

1.2.2 Mass loss in binaries

Mass loss effects are different in binary systems, since mass loss may be enhanced by the presence of the companion star, thus affecting the final structure of the star significantly. The mass transfer process is as follows: When the parent star reaches its Roche lobe limit, matter will be transferred to the companion star through a Roche flow. Depending on its intensity, this phenomenon can totally strip the hydrogen envelope of a star thus creating a Wolf-Rayet star, or can even remove the helium envelope, thus forming a CO star (Woosley et al. 2002). It is believed that the progenitor star of SN 1993J was in a binary system, which can explain how a 15 $M_\odot$ star had lost most of its hydrogen envelope. In more extreme cases the two stars will merge, since they had shared a common envelope for some period. One of the models for the progenitor of SN 1987A suggests a merger scenario to explain the observed properties (see Sect. 1.10).

1.2.3 Effects of mass loss

The evolution of a star is determined by its initial mass and metallicity (Z). These two parameters are critical for the mass loss throughout its life (in a single star). Thus a star with high initial mass and metallicity tends to experience higher mass loss during its lifetime and this effect scales as $\propto Z^{1/2}$ (Heger et al. 2003). Thus stars with low metallicity suffer less from mass loss, and end their lives with large helium cores and large hydrogen envelopes. The higher the metallicity and mass, the higher the significance of mass loss. The mass loss effect models presented below as parameters of mass and metallicity, are based on Heger et al. (2003), considering only non-rotating stars.

Stars with low metallicity in the mass range $10 - 25$ $M_\odot$ end their lives with massive hydrogen envelopes (≥ 2 $M_\odot$) and explode as Type IIP supernovae. In case the metallicity is low enough (see Fig. 1.3), stars in the mass range $25 - 40$ $M_\odot$, also explode as Type IIP supernovae. After the explosion, a neutron star is left at the centre. Stars with very high metallicities will experience high mass loss during their evolution, and at the end of their lives they retain very thin hydrogen envelopes (≤ 2 $M_\odot$). These stars explode as Type IIL supernovae, or Type IIb, if they have progenitors with mass above 25 $M_\odot$.

Such events form also black holes (see Fig 1.3) by fallback of ^{56}Ni, and they are fainter than normal.

To get Type Ib/c supernovae, the entire hydrogen envelope must be removed prior to the explosion. To get these types of supernovae, the progenitor star must have a high mass (≥ 34 M$_\odot$ Woosley et al. 2002) and metallicity (see Fig 1.3). Just like the Type IIL/b, many of these supernovae will form a black hole by fallback of matter so they are subluminous. A star with metallicity less than solar can explode as Type Ib/c, if the progenitor star has an initial mass $\sim$ 60 M$_\odot$. But to get mass loss of such extent, it is more likely for the star to be part of a binary than a single star. Another scenario that enhances mass loss is rotation. The models of Heger et al. (2003) in Fig. 1.3 do not assume rotation. If rotation is taken into account, then the lower, mass limit to get a Type Ib/c supernova for a star with solar metallicity goes down to $\sim$ 22 M$_\odot$ (Meynet & Maeder 2005).

In very massive stars ($100 - 140$ M$_\odot$) with low metallicity, pair instabilities take place in the form of violent pulsations. These stars form an iron core, and by the time of the explosion a substansial amount of mass is lost in the form of winds. The pulsations due to pair instabilities are so violent in stars $\sim$ $140 - 260$ M$_\odot$ that even a single pulse can disrupt the star completely, and no compact remnant is left behind. Finally, for the explosion of a star above 260 M$_\odot$ a black hole is expected (see Fig 1.3).

1.3 Explosion mechanisms

Gravity is the force behind stellar evolution. It is due to gravity that matter compresses, leading to star formation, and gravity is also responsible for triggering the conditions that lead to thermonuclear fusion. Through fusion, hydrogen is transformed to helium in the stellar core. When the core runs out of fuel, it contracts and helium burning takes place, leading to the formation of heavier elements such as carbon and oxygen. For stars with an initial mass $\geq$ 10 M$_\odot$ element synthesis continues until iron group elements are formed (Heger et al. 2003). Due to the fact that further element synthesis in the core stops, the core collapses destroying the star by launching a shock-wave.

Massive stars (M $\geq$ 9 M$_\odot$) are divided into distinct mass groups, where one can model their evolution. In the first group, we have the stars with initial mass between 9 - 10 M$_\odot$, while in the second those with initial mass above 10 M$_\odot$. A star in the mass range of 9 - 10 M$_\odot$ will not create an iron core, but in its final stage it develops an O-Ne-Mg core, which will eventually collapse, leaving behind a neutron star (Heger et al. 2003). The amount of ejected nickel is very small (< 0.015 M$_\odot$). At the moment of the explosion these starts still have a massive hydrogen envelope, and they explode as Type IIP supernovae. Stars heavier than 10 M$_\odot$, go through all the burning stages, and the only difference

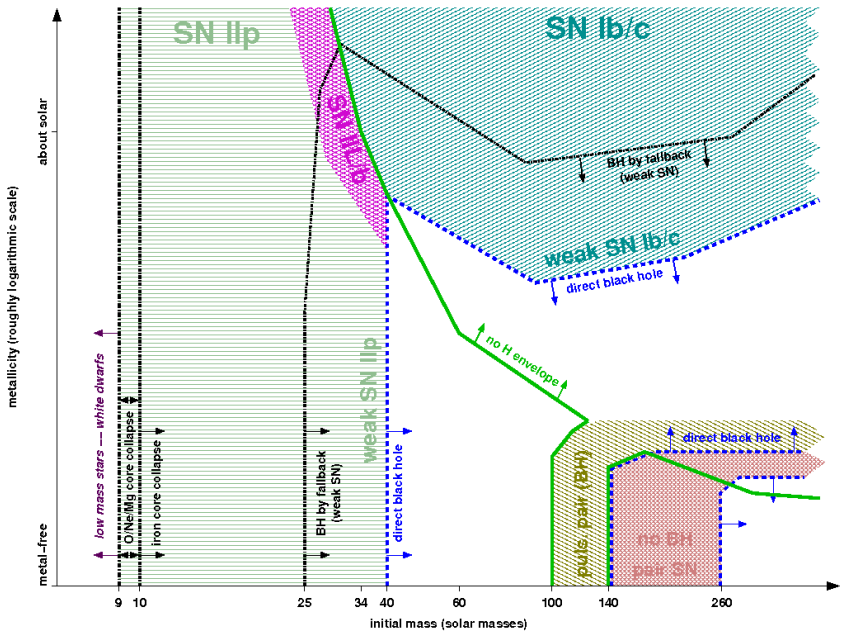

Figure 1.3: Supernova types from non-rotating stars as a function of their initial mass and metallicity. (From Heger et al. (2003)

in the outcome is the element distribution in their interior. As elements are synthesised in its interior, its structure resembles the different shells of an onion (Fig. 1.4). Starting from the surface and moving inwards, there is the unprocessed hydrogen envelope of the star. Helium is also present at higher abundance than at the zero age main sequence. Nitrogen, oxygen, and carbon is also present, which is a typical signature of the CNO burning, reaching the surface of the star due to convective mixing during the red super-giant phase. For nucleosynthesis the oxygen zone is the most important one. The mass of oxygen depends strongly on the initial mass of the star, and for a 25 $M_\odot$ star it is around 7 $M_\odot$, while for a 15 $M_\odot$ star it is around 3 $M_\odot$. Other elements with high abundances in this region are neon, argon, magnesium, silicon, and sulphur. The central 1.4 $M_\odot$ is dominated by iron group elements (i.e., iron, nickel), which are products of silicon burning.

The formation of an iron core marks the begining of the end for the star. This happens because the binding energy per nucleon in the iron group elements has its maximum value, thus no energy is released by nuclear fusion. Furthermore, there are two processes that remove energy from the core, thus making it unstable. The first one is electron capture, and the second is photodisintegration. At densities above 10^{10} g cm^{-3} (Woosley & Janka 2005) electron capture from protons increases the neutron number in the iron group nuclei, which

correspondingly reduces the electron pressure that supports the core stability. Futhermore at these conditions of pressure and temperature iron nuclei disintegrate into helium, a phenomenon that removes even more energy from the core. This makes the iron core to contract faster, thus increasing its density, which in turn permits further electron capture making the core even more unstable. Thus the core collapses nearly freely at a speed of 0.25c (Woosley & Janka 2005). This creates a neutron core of a radius of about 30 km, where the collapse is temporarly held by the repulsive component of the strong nuclear force.

At these conditions of density and temperature, most of the energy is released in the form of neutrinos. Neutrinos are scattered by both free and bound neutrons and protons. At this point the density is of the order 10^{12} g cm^{-3} and neutrinos are trapped, thus core collapse continues almost adiabatically. This happens because the diffusion time of neutrinos is longer than the dynamical scale of the collapse. The core continues to collapse till it reaches a density higher than nuclear ($\sim 2\times10^{14}$ g cm^{-3}), and at this point the infalling material starts to bounce backwards, due to the strong repulsive nuclear force. An effect of this is to send a shock wave outwards.

As the shock wave propagates outwards it loses energy, since it disintegrates the iron core into protons and neutrons. The free protons then capture electrons forming neutrons releasing neutrinos, which reduces the energy of the shock even further. According to the latest models (Janka et al. 2008), this causes a temporarily halt in the shock. This sets up an accretion shock inside the iron core as the infall of matter continues. Thus to have an explosion another process in needed to launch the shock wave.

A possible way to relaunch the shockwave and lead to an explosion, is the energy transfer from neutrinos in the area behind the accretion shock. In this case neutrinos from the inner core heat the post shock gas. This increases the density, and assuming that neutrinos can transfer a significant amount of their energy ($\sim$ 10%, Janka et al. 2008) enough pressure will be built up that can lead to an explosion. This mechanism is also known as the delayed explosion mechanism.

Another possible way that can lead to a successful explosion is to consider hydrodynamic instabilities. According to Blondin et al. (2003) a standing accretion shock instability can grow in the stellar interior, independently of the convective motions. Due to this, the accreted gas stays longer in the heated interior of the shock, and thus it can absorb energy from the neutrinos more efficiently. This eventually will relaunch the shock, leading to a supernova explosion. As the shock propagates outwards it suffers a smaller energy loss, since the density is significantly lower than in the core, and it will eventually emerge from the surface of the star.

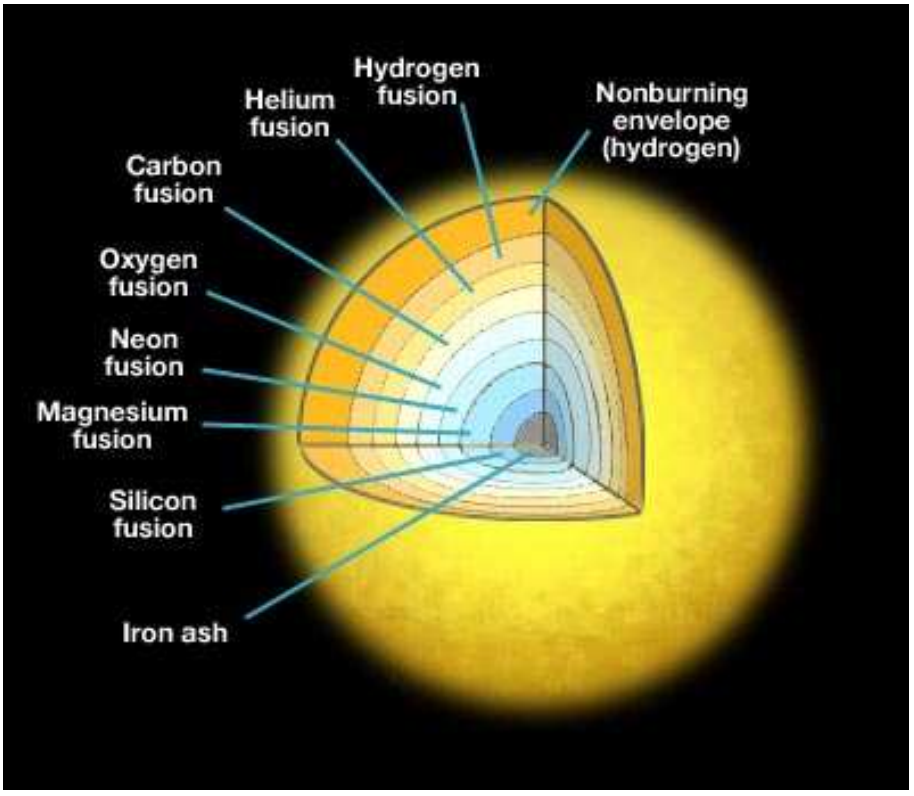

Figure 1.4: The structure of a massive star (according to elements) just before explosion. The relative sizes of the different zones are not to scale. (From Penn State University.)

1.4 Leftovers from the explosion

Supernova explosions make for a lot of interesting physics. Thermonuclear explosions destroy the star totally, and what is left after the explosion is an expanding remnant, which interacts with its surrounding medium, and eventually merges with it. Core collapse supernovae can leave behind them, apart from expanding gaseous nebulae, extremely compact objects (see also Sect. 1.2 & 1.3). A black hole will be formed only from very massive stars, while stars with lower mass are expected to form a neutron star (Heger et al. 2003, see Fig. 1.5 for details).

1.4.1 Neutron stars

The association of neutron stars with supernova explosions came shortly after the discovery of the neutron. Baade & Zwicky (1934) first pointed out the idea of neutron stars, that these would be objects with high density (close

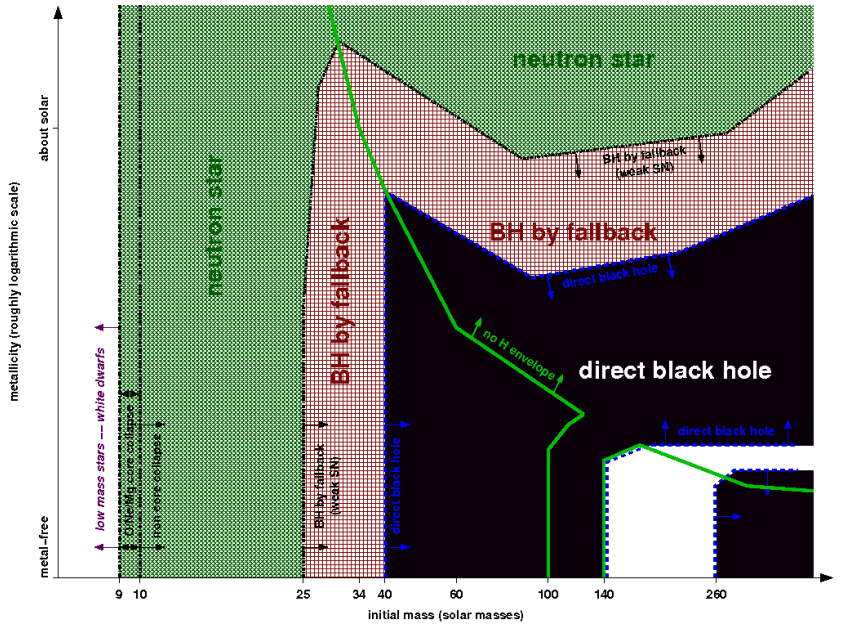

Figure 1.5: The resulted remnants from core collapse supernovae, as parameters of initial mass and metallicity. (From Heger et al. 2003)

to nuclear), with very small radius (in the order of a few km) and being much more gravitationally bound than ordinary stars. It was suggested that an object like this would be formed in a supernova explosion. The first models for neutron stars were made by Oppenheimer & Volkoff (1939) by assuming an ideal gas of free neutrons. The idea of neutron stars was almost ignored in the following years, until the discovery of X-ray sources. The interest became even stronger when the first pulsar was discovered. Gold (1968) proposed that pulsars are rapidly rotating neutron stars. The discovery of pulsars in the Crab nebula and later in Vela gave more support to this scenario. Neutron stars are believed to be energy sources that can power supernova remnants (SNR) or at least a fraction of their emission. There are two possible mechanisms through which a neutron star can provide power to the SNR. The first is the loss of rotational energy from the rapidly rotating neutron star, while the second is the decay of an extremely strong magnetic field that provides the electromagnetic power.

As an approximation for the structure of a neutron star, one can assume a degenerate gas consisting of non-interacting particles. In a more realistic model, a neutron star is divided into three zones. Starting from the surface and moving inwards, the outer crust consists of free electrons and free nuclei. The inner crust is composed of a superfluid of neutrons, mixed with electrons and nuclei. The inner part of the star is made of a superfluid of neutrons and nuclei.

In some models of neutron stars, a small core of free quarks is considered to exist. The upper mass limit of a stable neutron star, is 2.0 $M_\odot$ (Kiziltan et al. 2010), while its radius is $\sim$ 12 km (assuming a normal pulsar, see Kiziltan et al. 2010 for further details).

1.4.2 Black holes

The association of black holes with supernova explosions dates back to the late 30's when Oppenheimer & Snyder (1939) were the first to find that a sphere with the properties of a black hole will have no communication with the rest of the Universe. Black holes were reconsidered when realistic models of stellar collapse were created. It was Wheeler & Harkness (1968) who first gave the name black hole.

Stellar mass black holes have their origin in the cores of very massive stars (Heger et al. 2003, see also Sect. 1.2 & 1.3). The current model that describes the black hole formation is the collapsar model for long γ-ray bursts (MacFadyen et al. 2000). The black hole may form either promptly, or in a mild explosion, by fallback. In the latter case, the inner layers of the star initially move outward but lack adequate momentum to eject all the matter exterior to the young neutron star. Over a period of minutes to hours, $\sim$ 0.1 - 0.5 $M_\odot$ falls back onto the collapsed remnant, turning it into a black hole and establishing an accretion disk. A famous black hole candidate is Cyg X-1, for which the mass has been estimated to be 8.7 ± 0.8 $M_\odot$ (Shaposhnikov & Titarchuk 2007).

1.5 Supernova Remnants

A supernova remnant (SNR) is bounded by an expanding shock-wave, consisting of material ejected from the explosion of the parent star, and as time passes, by interstellar material that is swept along the way of the shock. They are created from both physical types of supernovae (core-colllapse & thermonuclear), with the differences being in the spectrum of the SNR, and the fact that core-collapse explosions in most cases leave behind them central compact remnants.

In terms of their morphology, SNRs are divided into three categories. The first contains all the shell type remnants (e.g., Cas A), meaning that their shape is roughly spherical. These remnants are characterised by emission of both radio and X-rays, with spectral indices $\alpha_\nu = 0.5 - 0.6$ suggesting synchrotron emission. The spectral index is defined as $F_\nu \propto \nu^{-\alpha_\nu}$, where ν is the frequency and F_ν the flux. The second category contains the plerionic rem-

Table 1.1: Young core collapse supernova remnants

SNR	SN type	Age (yrs)	Compact source	Period (ms)	B 10^{12} (G)[a]	Element[a] overabundance
SN 1987A	IIP	24	Black hole ?	-	-	O
Cas A[b]	IIb[f]	330	Weak		-	O, Si, N
PSR 0540-69[c]	IIP	800	Neutron star	50	5	O
Crab	IIP	957	Neutron star	33	4	He
Kes 75 [a]	Ib/c	1,000	Neutron star	325	48	-
3C58[a]	IIP	2,400	Neutron star	66	4	N
Vela	IIP	11,300[e]	Neutron star	89	3[d]	

[a] Chevalier (2005)

[b] Fesen et al. (2006)

[c] Lundqvist et al. (2010)

[d] Pavlov et al. (2001)

[e] Chen & Gehrels (1999)

[f] Krause et al. (2008)

nants. Plerionic means that the remnants have their centres filled, and that they are strong radio and X-ray emitters. They are distinguished from the shell type remnants by their almost flat radio spectra ($-0.3 \leq \alpha_\nu \leq 0$). The best known case of a plerionic remnant is the Crab nebula. The third and final category contains all the composite remnants. These display the morphological characteristics of both previous categories, with SNR 0540-69.3 in the LMC, being an instructive example.

Detailed studies have revealed the element abundances in many SNRs, thus allowing models of stellar evolution and nucleosynthesis to be confirmed. In Table 1.1, the basic information of some of the most studied young core collapse SNRs are shown. Vela is included in Table 1.1, to serve as an object in the transition phase from a young core collapse remnant, to a middle-aged remnant. It can be seen that remnants like Cas A, SN 1987A and SNR 0540-69 are rich in elements such as O and N, indicating massive progenitors. The fact that these remnants are rich in these elements, and that their ejecta have not mixed with the interstellar medium, can provide details of the nucleosynthesis that took place in the progenitor. Another feature of these category of young SNRs is that practically all of them (apart from Cas A and SN 1987A) contain a normal pulsar.

The articles in this thesis deal with observations of two young core SNRs, namely two of the most well studied objects in the sky, the Crab nebula and SN 1987A. The proximity of the Crab nebula and SN 1987A offers a unique opportunity to study the evolution of these supernova remnants in detail, allowing us to probe the late stages of stellar evolution of massive stars.

SN 1987A is a very young remnant, since its age is only 24 years, while the Crab is a young remnant ($\sim$ 957 years).

Studies of young remnants are of great interest. Through detailed observations the element abundances of the remnant can be estimated, thus extracting important information about the explosion, and the evolution of the progenitor star. They are ideal objects to study shock physics, and due to the presence of strong magnetic fields, they are ideal candidates for particle acceleration. As described above, young SNRs that arise from core-collapse supernovae should in most cases leave behind them compact objects. These compact objects create interesting physical systems, and in the case of a neutron star, a PWN is formed. Studies of PWNe provide important details on the emission mechanism, and evolution of neutron stars, which helps us understand the properties of nuclear matter.

1.5.1 Supernova remnants and the circumstellar medium of the progenitor

Circumstellar material plays an important role in the evolution of the star. As we discussed in Sect. 1.2, the amount of mass that is stripped from a stellar envelope determines the type of the supernova, and it has an influence on the subsequent supernova evolution. A dense circumstellar medium (CSM) can also change the type of the supernova (see Sect. 1.1) that is observed. Observations of supernova interacting with its CSM can provide important information on the mass loss and evolution of the massive star. A feature that indicates that the gas in the CSM region is progenitor related, and not ISM related, is its composition. The [N II]/Hα ratio is usually high (e.g. $\sim$ 1.9 for the southern outer ring of SN 1987A, see Paper III, and 2.1 for the bipolar outflow of Sher 25, Brandner et al. 1997), which can only be due to matter ejected from the star. Considering that Sher 25 (B1.5 I) is still evolving, and that it is a Galactic object (allowing observations with higher spatial resolution), offers a unique opportunity to study an object similar to the SN 1987A progenitor (B3 I), and extract important information about its mass loss history.

1.6 Remnant evolution

The evolution of a SNR can be divided into four different phases. These are known as: The free expansion phase, the Sedov-Taylor phase, the snowplow phase, and finally the momentum conserving phase where the remnant merges with the interstellar medium. The first phase (free expansion phase) starts when the shock-wave generated from the supernova explosion reaches

the surface of the star. In this stage roughly all the material of the SNR consists of material that comes from the stellar ejecta. The average velocity of the ejecta is:

$$V_{SNR} \simeq (\frac{2E_0}{M_{ej}})^{1/2} \tag{1.1}$$

The outer parts of the ejecta of a supernova are expected to be slowed down at its early phase due to interaction with the CSM, but this does not really affect the bulk of the ejecta. During the free-expansion phase a possible pulsar wind nebula (PWN) expands supersonically into the ejecta, and in the SNR during this phase there are four shocks present and two contact discontinuities (see Fig. 1.6). The shock closest to the centre comes from the pulsar wind (pulsar wind termination shock), then we encounter the first discontinuity which separates the shocked pulsar wind material from the ejecta material that is shocked by the SN shock. The second shock comes from the PWN which bounds the PWN. A reverse shock is also present in the SNR, and after this there is the second discontinuity which separates the shocked supernova ejecta from the shocked ISM (or CSM). The fourth shock is the SN shock which bounds the whole SNR/PWN system.

When the swept up mass of the ISM exceeds the ejecta mass, then the SNR enters its second phase of evolution known as the Sedov-Taylor phase (Sedov 1959). At this point the reverse shock has driven deep inside the remnant and it reheats the stellar ejecta. As a direct effect of this, the local sound velocity increases. Since the local sound velocity increases during this phase by reheating from the reverse shock, the PWN expands sub-sonically into the remnant (Van der Swaluw et al. 2001). The radius of the PWN can be associated with the contact discontinuity that separates the pulsar wind material from the ejecta of the progenitor star.

During this phase there are two shocks and two contact discontinuities that are present. The first shock is the pulsar wind termination shock. This is followed by the first contact discontinuity which separates the shocked pulsar wind material from the shocked ejecta that bounds the PWN. The second contact discontinuity separates the shocked material of the SNR from the shocked material of the ISM. Finally, at the boundary of the SNR/PWN system, there is the shock from the SN explosion.

The timescales of these phases vary significantly. The free expansion lasts for a period between 100-1,000 years, while the Sedov-Taylor phase can last around 10,000 years (Van der Swaluw et al. 2001). During the Sedov-Taylor phase, the internal pressure balances the ram pressure of the swept up material, and the expansion rate is still controlled by the kinetic energy conservation. The Sedov-Taylor solution is a fairly accurate way to treat the evolution of a SNR as long as energy is conserved and radiation losses are insignificant.

When radiation losses become important in the shell of the swept mass, then the remnant enters its next phase known as the snowplow stage. At this point

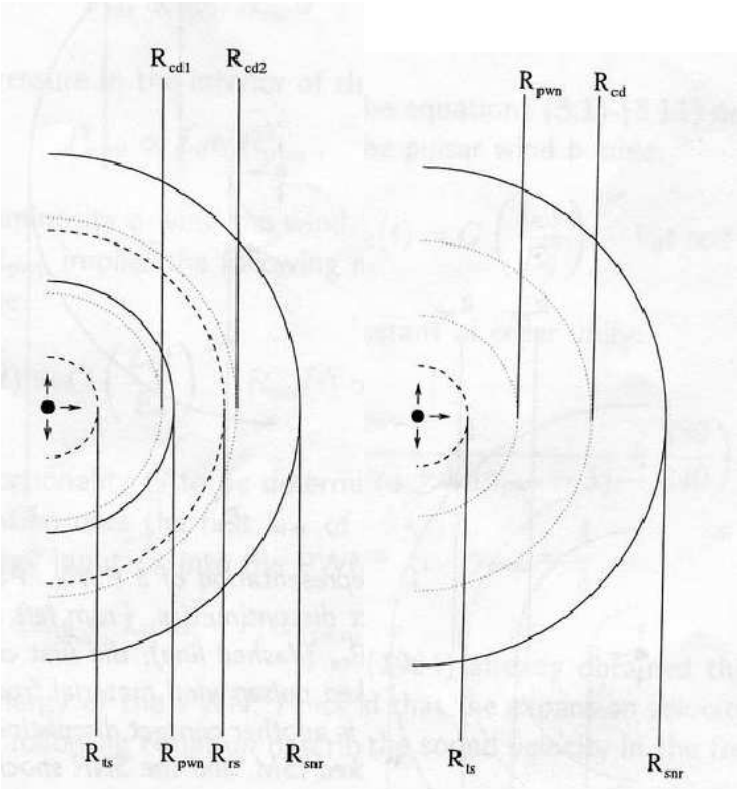

Figure 1.6: Left panel: Schematic representation of Crab-like SNR in the free expansion phase. Starting from left to right there is the pulsar wind termination shock R_{ts} (dashed line), followed by the first discontinuity R_{cd1} (dotted line) that separates shock pulsar wind material from shocked ejecta. The second shock is the PWN shock R_{pwn} that bounds the PWN. In the SNR there is the reverse shock R_{rs} (dashed line), followed the second discontinuity R_{cd2} (dotted line) that separates shocked ejecta from shocked ISM. Finally, the fourth shock, is the SNR shock R_{snr} (solid line) which bounds the outer PWN/SNR. Right panel: Schematic reprentation of a Crab like remnant in the Sedov phase. Starting from the left there is the pulsar wind termination shock R_{ts} (dashed line), followed by the first discontinuity R_{pwn} (dotted line) that separates the shocked pulsar wind material from the shocked ejecta that bounds the PWN. The next discontinuity that follows R_{cd} (dotted line) separates the shocked ejecta from the shocked ISM, which in turn is followed by the SNR shock R_{snr} which bounds the PWN/SNR. (From van der Swaluw et al. 2001)

of evolution, the mass that is swept up collapses to a thin dense layer, while the interior of the SNR expands adiabatically. The pressure from the interior pushes the shell through the ISM. As a result of this, the internal energy is not constant.

The final stage sets the beginning of the end for the SNR since it will then merge with the ISM. A remnant will enter this phase when the pressure in the interior of the SNR becomes comparable with pressure of the ISM. In this case, no force acts on the shell of the SNR which means that momentum is conserved, while the shock continues to sweep interstellar gas. This stage is known as the momentum-conserving snowplow phase and after this the remnant merges completely with the ISM, and it leaves behind it a cavity of higher temperature than the surrounding ISM. The time scale for this to

happen is typically around 750,000 years after the supernova explosion (Cioffi 1990).

1.7 Pulsar Wind Nebulae

Apart from studying young core-collapse SNRs, this thesis also deals with studies on PWNe. A PWN is a nebula powered by the pulsar wind of a pulsar. This wind is composed of charged particles accelerated to relativistic speeds by the rapidly rotating superstrong magnetic field of the spinning pulsar. This electromagnetic radiation can be observed as synchrotron and inverse Compton emission. Goals of studying PWNe are to improve our knowledge of neutron stars, and in turn, matter at nuclear densities. Additionally, an environment like that of a PWN, helps us to understand the relativistic effects of extreme electromagnetic and gravitational fields in fast moving particles and gas.

In terms of classification schemes, PWNe are divided into groups based on their morphology. Using X-ray data from Chandra, Kargaltsev & Pavlov (2008) made a classification of all known PWNe. In the first category, we find all the Crab-like PWNe, in the second all the bowshock tail PWNe (e.g., the Guitar nebula), and in the last, all the irregular PWNe. The Crab-like PWNe are the most studied cases, and various magneto-hydrodynamic models (Del Zanna et al. 2004, 2006) have been suggested to explain their properties. Bowshock tail PWNe have shapes that are affected by the high speed of the pulsar's motion. These pulsars move at velocities $\geq$ 500 km s^{-1}, and eventually they escape from their host PWN, and move into the supernova ejecta thus forming a comet like PWN. Finally, according to Kargaltsev & Pavlov (2008), the irregular PWNe are still a mystery in terms of their formation.

1.8 The Crab nebula

The Crab Nebula is one of the most studied objects in the sky. Located in the constellation of Taurus, it is associated with SN 1054, a supernova explosion that was observed by Chinese and Japanese astronomers. It is located at a distance of around 2.0 $\pm$0.5 kpc (Kaplan et al. 2008), and lies at a distance of around 200 pc from the galactic plane (Sankrit et al. 1998). The Crab claims many "first" detections, since it was the first extra solar radio source, X-ray source, and synchrotron radiation source (Trimble 1985). The Crab pulsar sits in the centre of the nebula, and is responsible for powering the nebula (see Fig. 1.7). Together with the synchrotron nebula, and the filaments they form the Crab nebula. The term filament has been used to refer to the macroscopic

structures seen in ground based images of the Crab. These structures constitute discrete units in the nebula, results of hydrodynamic instabilities.

1.8.1 Identifying the progenitor star

Unless there are direct observations prior to the explosion, we need indirect evidence to identify the progenitor star of a supernova. Detailed spectroscopic information can provide important information on the element distribution of the remnant, thus helping us to understand the nature of the progenitor star. Likewise, mapping out the CSM or identifying a compact object helps in constraining the progenitor. For example, the presence of a pulsar in the Crab nebula clearly shows that the Crab was a core-collapse supernova, and from its hydrogen rich spectrum that it was a Type II explosion. Furthermore, studies on the element abundances in the nebula suggest that the progenitor had a mass lower than 13 $M_{\odot}$ (Nomoto 1985). In particular, the He/H ratio measured in the Crab could be an indication that the progenitor is within the 8 - 13 $M_{\odot}$ mass range (Nomoto 1985), but in order for this to be true, a star like this has to lose much mass in the form of winds. Furthermore, the abundance of carbon in the Crab nebula is small and is also consistent with stars between 8 - 9.5 $M_{\odot}$ (Nomoto 1985). All this indicates that the Crab nebula was the result of a Type IIP explosion of relatively low mass. Also from arguments analysing historical data, Sollerman et al. (2001) argue that SN 1054 did not show evidence against this hypothesis.

1.8.2 Structure of the Crab nebula

The Crab nebula is located in a low density region of the Galaxy. So far there is no direct evidence of interaction of the ejecta with the ambient material. This means that the filaments of the nebula are uncontaminated by interstellar matter. By way of a brief description and starting from its interior and moving outwards, the Crab consists of the Crab pulsar, the Crab synchrotron nebula, and a bright shell of thermal gas. A fourth and yet not detected faint structure is expected to exist around the visible Crab, expanding at a high velocity ($\geq$ 2500 km/s). The detection of this component was the main task during my thesis, and is discussed in Papers I & IV.

1.8.3 The Crab pulsar and its pulsar wind nebula.

The Crab pulsar is one of the most studied pulsars, and since its discovery in 1968 (Staelin & Reifenstein 1968), it has been studied from radio to γ-rays.

It was also the first detected pulsar at optical bands (Cocke et al. 1969), and it acts as model for all the plerions. The immediate environment of the Crab pulsar is a really interesting region consisting of jets, a torus of X-ray emission (Aschenbach & Brinkmann 1975), small scale variation in polarization and spectral index (Bietenholz & Kronberg 1992), and complexes of arclike structures known as wisps (Scargle 1969).

Activity in the environment of the Crab pulsar and its surroundings has been reported decades back, by Lampland (1921) and by Oort & Walraven (1956). A very comprehensive study was undertaken by Scargle (1969), who found that the so called wisps may show relativistic motion, but conversely always seem to be more or less located at the same position. The use of HST has provided some of the most detailed images of the Crab pulsar and its surroundings. High resolution surveys were conducted by Hester et al. (1995; 2002), using WFPC2, complemented with X-ray data from ROSAT and Chandra. The most outstanding discovery is the presence of two knots that are situated $0\farcs65$ and $3\farcs8$ southeast of the pulsar. The X-ray data have also shown many other knots around the pulsar that show variability with time. Further observations from optical to IR have revealed that the wisps and the nearby knot display red spectra (Sollerman 2003), and that they also show variability on kilosecond timescale (Melatos et al. 2005).

For a brief discription of the immediate environment of the Crab PWN, we note that the knot $0\farcs65$ southeast of the pulsar is aligned with the X-ray/optical jet and that it has an elongated shape. Its nature is still not clear, but it can be attributed to a shock wave or an instability feature in the jet flow. The arc like features known as "wisps" appear to have an outward motion and X-ray observations report velocities of up to 0.5c. There are two possible ways to explain their existence. The first is that the wisps exist due to an ion dominated wind that suffers cyclotron instability at the termination shock (Spitkovsky & Arons 2004), or that they are the result of synchrotron cooling instabilities in a flow that is undergoing a transition from being particle dominated to being field dominated (Hester et al. 2002). Finally, the nature of the torus is still not clear, but it is believed that its nature is due to Doppler boosting and relativistic aberration (Mori et al. 2004).

Paper II was based on optical and infrared observations of the Crab PWN, where the task was to monitor the emissivity and dynamic variations of the Crab PWN. Additionally we checked whether or not the nearby knot has a proper motion with respect to the pulsar, or if they move together as a whole system.

1.8.4 The filaments and the expanding nebula

The synchrotron nebula is surrounded by the thermal filaments. The latter are composed of ejecta from the supernova. Observations have shown expan-

sion velocities that mainly range between 700-1800 km s^{-1} (Charlebois et al. 2010, Paper IV). In a few directions and most notably so for the so called "chimney" in the north, velocities extend to beyond 2000 km s^{-1}. Spectra have shown hydrogen Balmer lines, and other emission lines that range from H_2 (Graham et al. 1990) to C IV λ1549 (Blair et al. 1992). Spectroscopic studies and plasma diagnostics (Fesen & Kirshner 1982) have revealed that the [S II] $\lambda\lambda$6716, 6731 line ratios indicate densities between 600-1700 cm^{-3} across the nebula, and that the [O III] temperature is between 11,000-18,000 K, while the [N II] temperature is 9,500-13,500 K. These temperatures point to photoionisation rather than shocks as the main excitation mechanism.

Using HST, Hester et al. (1996) and Sankrit et al. (1998), found that the filaments break up into many smaller concentrations of emission, and argued that the filaments of the Crab are the result of Rayleigh-Taylor (R-T) instabilities between the synchrotron nebula and the denser ejecta which it pushes. The filaments form finger-like structures with a width of $\sim$ 1", while their length ranges from $\sim$ 1" up to $\sim$ 20". An interesting feature first observed by Gull & Fesen (1982) is the presence of a thin and faint "skin" of high ionisation, mainly seen in [O III] that seems to surround the Crab. This feature is believed to trace the interface between the synchrotron nebula, and the ejecta. It also connects the tops of the R-T fingers, protruding radially inward to the PWN. Sankrit & Hester (1997) intepreted this feature due to the presence of a cooling region, behind a shock that is driven by the pressure of the synchrotron nebula, into an extended remnant of freely expanding ejecta. Finally, another interesting feature in the Crab is the presence of an asymmetry, seen in the north west region of the nebula. There the [O III] "skin" is practically not present, or is too faint to be detected. This area seems to coincide with the direction of the proper motion of the Crab pulsar. This is also the only part of the nebula (except the chimney) where the synchrotron nebula extends beyond the filaments, suggesting that there is a variation in the density of the ejecta into which the nebula expands.

1.8.5 Problems with the Crab

The hydrogen rich spectrum, and the presence of a pulsar, may be the direct evidence that the Crab was a Type II explosion, but the kinetic energy and the mass of its ejecta are far from canonical values. From observations (Fesen et al. 1997), the measured mass of the observed nebula is only 4.6 ± 1.8 $M_\odot$. To this, one should add the mass of the pulsar (i.e. ~ 1.4 $M_\odot$). This mass, and the average velocity of the filaments corresponds to a kinetic energy of $\sim 10^{49.5}$ ergs (Hester 2008), a factor of $\sim$ 30 less than the canonical value. Therefore, a faint and yet not detected component (Chevalier 1977) must exist that carries the missing mass and kinetic energy of the Crab, if SN 1054 was a normal supernova. This must lie outside the observed remnant, and it is expected to

interact with the surrounding gas just like SNR 0540-69 in the LMC. Various surveys have been performed from radio to X-rays (see Fesen et al. 1997, and references within), but no emission related to the Crab has been detected. This, however, may only be due to the very low density around the nebula, so the interaction between the hypothetical shell and the ISM is too weak to detected (Romani et al. 1990).

As we noted above, indirect evidence for a fast shell comes from the [O III] "skin" (Sankrit et al. 1998). Perhaps the best direct evidence for a shell around the Crab come from the far-UV spectroscopic studies of Sollerman et al. (2000). An absorption feature in C IV λ1548, which extends out to 2500 km s^{-1} was detected, a feature predicted by photoionisation models by Lundqvist et al. (1986). A lower limit of the shell mass was estimated at $\sim$ 0.3 $M_{\odot}$ with a kinetic energy of $\sim 1.5 \times 10^{49}$ ergs. The C IV data are also compatible with normal kinetic energies of core-collapse supernova. Inspired by this, we decided to search for a halo around the Crab. To get a complete view, we used both photometry and spectroscopy. In Paper I, we present our results from the photometric studies, where we used deep Hα imaging, while in Paper IV we present our spectroscopic study, where we tried to find fast moving gas components mainly in the form of [O III] emission and Ca II absorption lines. The task was to detect a halo that can carry the missing mass and kinetic energy of the Crab. The detection of such a halo with mass $\geq$ 2 $M_{\odot}$ moving at a speed $\sim$ 2500 km s^{-1}, will let us check whether the Crab was a normal supernova explosion as described by Heger et al. (2003) and Janka et al. (2008), or it was a low energy explosion as described in Kitaura et al. (2006). We should mention here that Clark et al. (1983) have presented a spectrum of the Crab with higher resolution than our ALFOSC spectrum, focusing only on the [O III] doublet. It should be mentioned here that high resolution spectroscopy is not ideal for search features like the Crab halo, because disentangling the possible halo from the filaments becomes difficult.

1.9 SN 1987A

Perhaps the most famous supernova after the Crab is SN 1987A. Located in the Large Magellanic Cloud (LMC) at a distance of 51.4 kpc (Panagia 1999), it was the first naked-eye supernova since SN 1604. This presented a unique opportunity to study a supernova from its birth throughout its evolution up till the present. SN 1987A was unique in many ways, since its progenitor Sk-69°202, a BSG (B3 Ia), with a main sequence mass $\sim$ 20 $M_{\odot}$, was observed prior to the explosion (Walborn et al. 1989). This caused much surprise, since it did not agree with general concensus that a star explode as a supernova while in its RSG phase. On the contrary, the progenitor star of SN 1987A was a BSG. From the lightcurve of SN 1987A it was found that

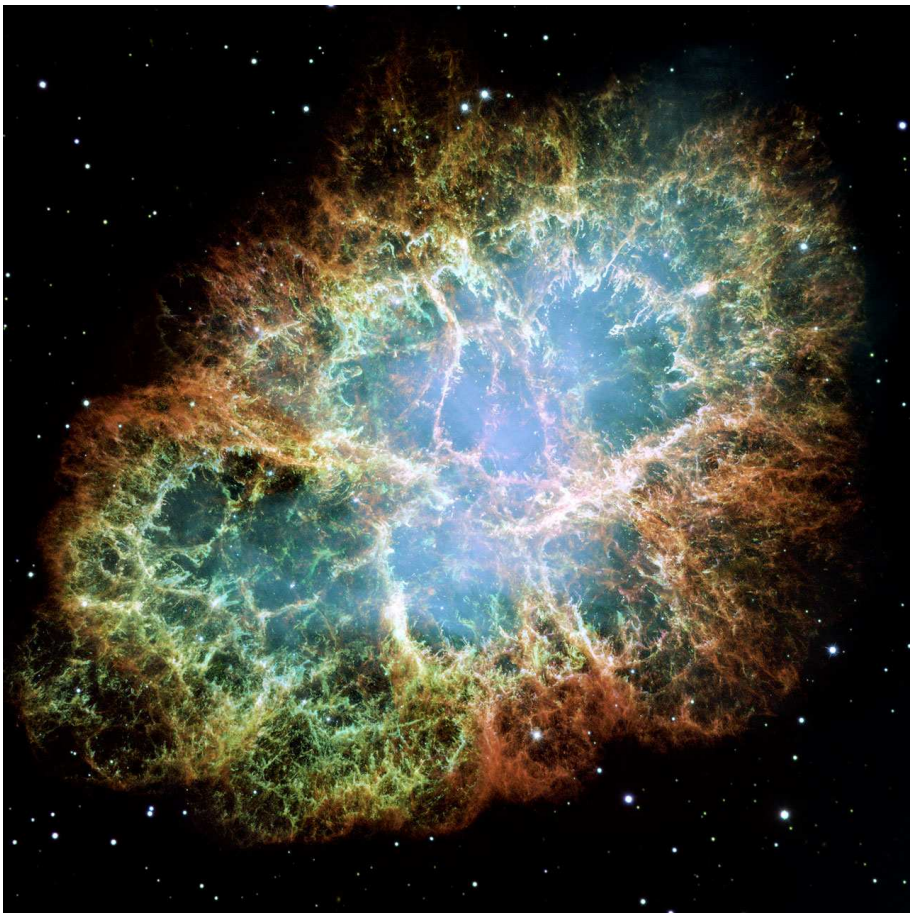

Figure 1.7: Image of the Crab nebula taken with WFPC2 onboard HST. The filaments that surround the synchrotron nebula are seen, together with the [O III] "skin" around them. The emission of [O III] (F502N) is shown in red, [S II] (F631N) is seen in green, while the [O I] emission is in blue (F631N). (Courtesy of STSCI).

the progenitor was compact, since most of the thermal energy from the explosion was lost during the adiabatic expansion of the supernova. That made SN 1987A rather dim with respect to other Type II explosions. SN 1987A was classified as a Type IIP supernova, since it displayed a plateau phase for a period of $\sim$ 120 days. However, contrary to normal Type IIPs, the plateau was not powered by hydrogen recombination, but by radioactive decay. Apart from the opportunity of extensive studies, SN 1987A was unique also for another reason, namely the first detection of non-solar neutrinos. This confirmed the models for the core-collapse mechanism of massive stars. The only factor that is still missing to complete the picture of a normal Type II supernova explosion, is the detection of a compact source. So far none has been detected,

and Graves et al. (2005) have set an upper limit of $\leq 10^{34}$ ergs s^{-1} for any compact source.

1.9.1 Models for the progenitor star

Modeling of SN 1987A (Arnett et al. 1989) suggests a progenitor with initial mass around 20 $M_{\odot}$. This compares well with models based on the early emission by Blinnikov et al. (2000) and Utrobin (2005), which suggest an ejected mass of M_{ej} = 18.0 $\pm$ 1.5 $M_{\odot}$, and a released kinetic energy for the ejecta of E_{ej} = 1.50 $\pm$ 0.12 $\times$ 10^{51} ergs. Fransson & Lundqvist (1989) showed that the outer layers were rich in CNO material and helium suggesting that material from the core had been mixed with matter in the outer envelope. Over the past twenty years various models have been suggested to explain the progenitor of SN 1987A. These are divided into two categories. Those that evolve a single star, and those that evolve a binary system.

Starting with single star models, some initial models (Truran & Weiss 1987) considered a low metallicity star. According to this hypothesis, the star will never enter the RSG phase. This, however, does not agree with the colour indices of the nearby stars in the LMC. A more realistic model that was also able to explain the RSG phase of SN 1987A, and the change to a BSG prior to the explosion, was suggested by Washimi et al. (1999). They also tried to explain the origin of the triple ring system that surrounds SN 1987A. Hence the ring system was formed due to a BSG wind pushing on the RSG wind. This idea dates back to the models of Blondin & Lundqvist (1993) and Martin & Arnett (1995). In general the main problem with single star models (i.e., Langer 1991) is the fact that they cannot easily explain the overabundance of nuclear processed material.

Since we know that the progenitor of SN 1987A was a BSG star, the possibility that the explosion resulted from a binary system looks rather attractive, since it allows for a star to explode as a supernova in its BSG phase. The simplest case is to assume a star that accrets matter till it explodes (Podsiadlowski 1992). Through accretion of mass the high CNO abundancies of SN 1987A can be explained. Additionally, the transferred angular momentum due to accretion, made the progenitor star to rotate at a faster pace at the final stages of its life. This excess of angular momentum can provide an explanation for the rotational symmetry of the ring system.

Another possible way to explain the explosion of SN 1987A involves again a binary system, only this time the two stars merge (Morris & Podsiadlowski 2007). According to this model, it is assumed that two stars with initial masses of $\sim$ 15 $M_{\odot}$ and $\sim$ 5 $M_{\odot}$ form a binary system. Due to the large mass ratio, the mass transfer in the system is not stable and eventually leads to the formation of a common envelope, where eventually the two stars merge. During the common envelope phase the star displays the properties of a RSG, while

after the merge, as it shrinks, it later becomes a BSG star again. This model could possibly also explain the formation of the triple ring system. According to this model, the material of the rings was ejected from the progenitor star $\sim$ 20,000 years ago.

1.9.2 The ring system of SN 1987A

The triple ring system (see Fig. 1.8) that surrounds the supernova debris has perhaps provided the most spectacular feature seen in SN 1987A. Emission from the rings was detected in both the optical (Wampler et al. 1988), and as UV lines (Fransson & Lundqvist 1989). Responsible for the ionisation of the triple ring system, was the UV flash that accompanied the shock breakout from the supernova explosion (Fransson & Lundqvist 1989). Observations have shown that the material in the rings is nitrogen rich confirming their association with the progenitor star of SN 1987A. The three rings are elliptical in shape, with the equatorial ring (ER) centred on the supernova, and the two outer rings (ORs), centred to the north and south of the supernova, perhaps forming an hour glass structure. The ER is inclined by 43° (Sugerman 2002, 2005), and Crotts et al. (2007) determined that the ER has a radius of 0.6 ly and that it is expanding with a velocity of 10.3 km s^{-1}. The northern outer ring (NOR) is located at a distance of 1.92×10^{18} cm from the explosion centre, and it is inclined by 45° towards the Earth, while the southern outer ring (SOR) lies at a distance of 1.85×10^{18} cm from the explosion centre, and it is inclined by 38° away from the Earth. Both ORs have similar radii (2.5 times the inner ring's radius), and they both expand with a velocity of $\sim$ 20 km s^{-1}. Kinematics observations (Crotts & Heathcote 2000) suggest that both the ER and the ORs were created $\sim$ 20,000 years ago, by matter ejected from the progenitor star. This fits the modeling of Morris & Podsiadlowski (2007).

Lundqvist & Fransson (1996) estimated the element abundances and gas densities for the ER, confirming the association of the ER with the progenitor. They found densities for the ER varing between 6×10^3 cm^{-3} to 3.3×10^4 cm^{-3} and derived also the following relative abundances: He/H = 0.25 $\pm$ 0.05, N/C = 5.0 $\pm$ 2.0 and N/O = 1.1 $\pm$ 0.4, with an overall metal abundance (i.e., C, N and O) of 0.30 $\pm$ 0.05 times solar. The nitrogen enrichment of the ER suggests that the progenitor star was in a post He core burning phase at the time of the explosion (Podsiadlowski 1992). Since 1999 (Garnavich et al. 1999) the supernova ejecta have started to interact with the ER. This interaction has increased in strength, which is seen in relative fluxes of the narrow line emission from photoionised gas and the broader shock excited lines. In terms of gas temperatures in the ER these vary, significantly, depending on whether the gas is shocked or not. Thus for the unshocked the gases temperatures are similar to the OR temperatures, i.e., 10,000 K - 30,000 K (Gröningsson et al. 2008), while for the shocked gas the temperature can be as high as $\sim 10^6$ K

initially (Gröningsson et al. 2008). A good review of the evolution of the ER is presented by Mattila et al. (2010), where a detailed discussion is given for element abundances and gas densities.

The ORs were first revealed by Wampler et al. (1990), followed by detailed HST observations (Burrows et al. 1995). Crotts et al. (2000) reported a stucture that may possibly connect the ORs with the ER, but a feature like that can be due to dust or reflections from the ER and the supernova. Maran et al. (2000) showed that the surface brightness of the ORs is only 5 - 15 % of that of the ER, leading to similar density differences. Maran et al. (2000) found densities of the order 1000 - 2000 cm^{-3}, slightly higher than the reported values of Panagia et al. (1996) that reported densities $\sim$ 800 cm^{-3}. Finally Maran et al. (2000) estimated gas temperatures in the ORs which are $\sim$ 11,000K for the [N II] and $\sim$ 22,000K for the [O III] emitting gases.

The motivation for Paper III, was to study the emission closer, and to derive the temporal changes of important emission lines. We used optical data from the HST (WFPC2 & ACS) covering a period of almost ten years, together with spectra from FORS1 and UVES from VLT with a time gap of almost seven years. The HST data were used to check the evolution of various emission lines (i.e., [O III], [N II], and Hα) through the creation of lightcurves, while spectroscopy was used to estimate the evolution of the plasma properties (i.e., gas & temperature), of the emitting gas.

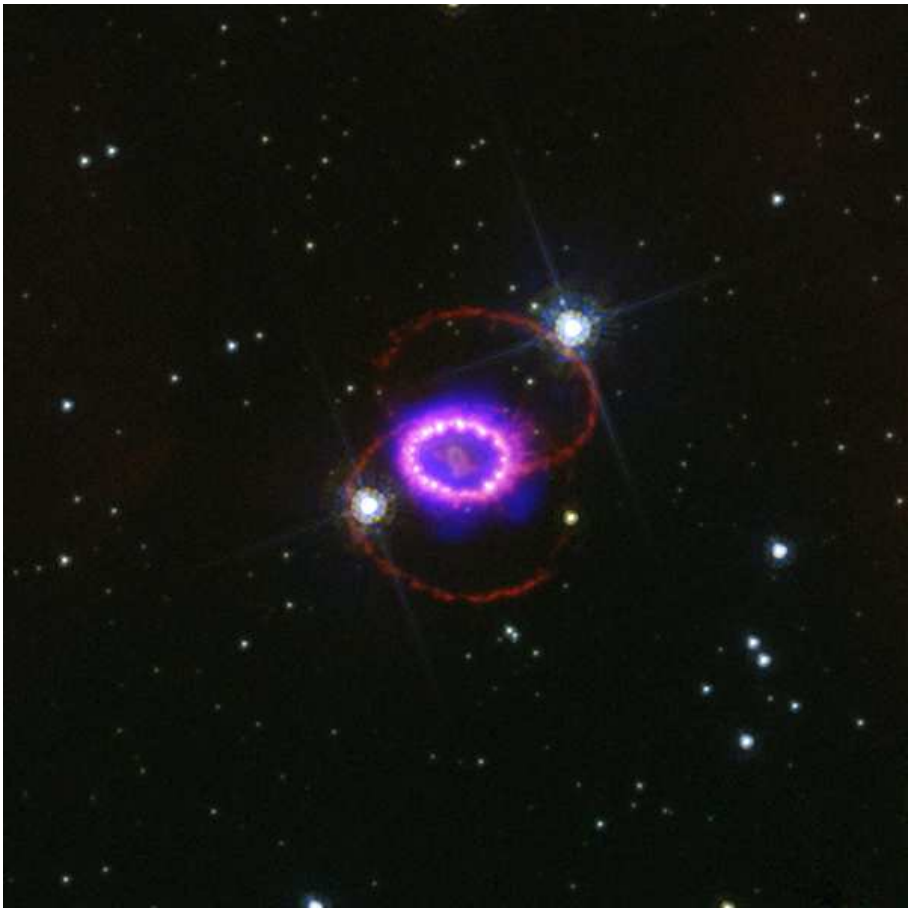

Figure 1.8: Combined image of SN 1987A in X-rays (Chandra) and optical (HST). The X-ray emission (blue) is really prominent, due to the interaction of the ejecta with the ER material. Another feature of the interaction between the ejecta and the ER is the presence of the numerous bright spots on the ER. The ORs centred to the north and south of supernova can also be seen. The image is 12 arcminutes across (From Zhekov et al. 2006).

Part II:
A possible halo around the Crab nebula

2. A possible halo around the Crab nebula

As outlined in Sect. 1.8.5 a fast moving halo around the nebula that carries the missing mass and kinetic energy could make the Crab a more normal supernova explosion. In particular, we expect a halo with a mass of ≥ 2 $M_{\odot}$ and speed up to 5000 km s^{-1}. In Papers I and IV we tried to find such a halo using photometry (Paper I), and spectroscopy (Paper IV). My contribution to these articles was in data reduction and data analysis. The models that we base the halo papers on are the work of my supervisor Peter Lundqvist. I also thank Mischa Schirmer for providing a pipeline for the reduction of the WFI data, and also assisting in the construction of PSF models we used in our analysis.

2.1 Results and Analysis

2.1.1 Photometry

In our effort to detect the halo we used two telescopes. The first dataset came from the Wide Field Imager (WFI) on the 2.2m telescope at ESO/La Silla, while the second came from the MOSaic CAmera (MOSCA) at the 2.56m Nordic Optical Telescope on La Palma, Spain. For both datasets we came across the same problem. The detected Hα haloes are not of real nature, but due to scattered light from the nebula (and the nearby stars). The measured profiles in the case of WFI extend out to 2.7 arcminutes, while the profile from MOSCA extends out to 1.3 arcminutes (see Fig. 2.1). The measured brightness is much higher than expected from theory (Lundqvist et al. 1986), and in both cases their peak value was higher than the upper limit Fesen et al. (1997) have set from spectroscopic studies. To check the extent of the effect we constructed models (for more details see Paper I) of the point spread function (PSF), which were convolved with the images with the hypothetical halo removed. The various PSF models were made using bright isolated stars from the images, and for the WFI the extending radius of the PSF was out to 2 arcminutes, while for the MOSCA data 1.3 arcminutes. We then compared the detected haloes from WFI and MOSCA with those created from the PSF convolution. The results can be seen in Fig. 2.2, from where it can be seen that scattered light dominates what was initially thought to be a halo. Still a halo with a peak flux up to 2×10^{-7} ergs s^{-1} cm^{-2} sr^{-1} could be accommodated

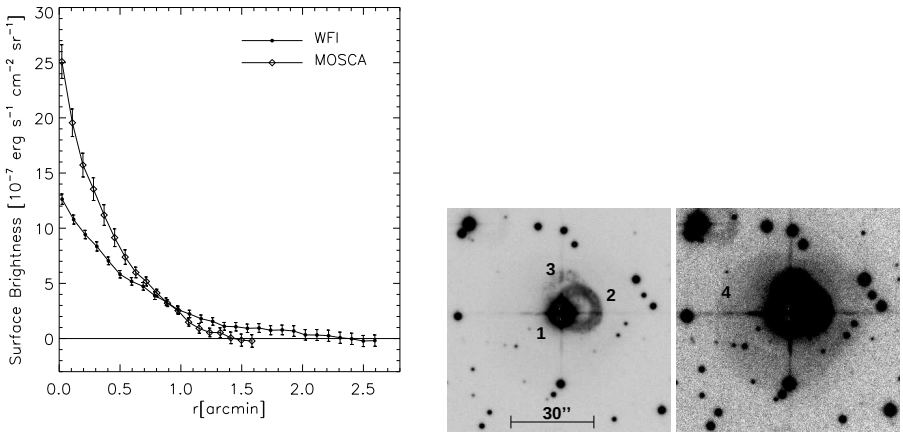

Figure 2.1: Left panel: The observed halo profiles. They fall off following power laws with slopes of -0.88 (WFI) and -1.12 (MOSCA). Right panel: Illustration of the WFI filter ghosts. The core of the PSF is labelled as 1, followed by three filter ghosts of decreasing intensity, labelled 2-4.

within error, but due to the extent of the PSF contamination and the lack of an accurately constructed PSF model (see below) no safe statement can be made.

2.1.2 Spectroscopy

Apart from photometric observations, we made a second attempt to solve the mysterious nature of the Crab. In our second effort we tried to search for fast moving components in the spectrum of the Crab. Therefore we again used two different telescopes, having two aims in mind. Thus we focused on the detection of fast moving components looking for broad Hα profiles, using a FORS1/VLT spectrum, and on the [O III] emission and the Ca II absorption line doublets, using an ALFOSC/NOT spectrum. The mixing of the Hα line with its neighbouring [N II] $\lambda\lambda$6548, 6583 lines, together with the low S/N ratio and resolution of the FORS1 spectrum did not allow us to make any estimates on broad components of the Hα profile. Thus more attention was paid to the ALFOSC spectrum, since the [O III] lines are isolated from any other strong emission line, plus that there we had the chance to also check for fast absorption components in the Ca II $\lambda\lambda$3934, 3968 absorption lines. This was done to compare with the C IV $\lambda\lambda$1548, 1551 line absorption in Sollerman et al. (2000), where a blueshifted absorption feature extending out to - 2500 km s^{-1} was detected. From the emission lines of [O III], the highest velocity $\sim$ 1800 km s^{-1} was found north of the pulsar, while on average the [O III] velocities are between -1200 to 1200 km s^{-1}. The Ca II search was not fruitful either. Starting with the λ3934 absorption line, a blueshifted feature out to $-$1150 km s^{-1} was measured and attributed to the Crab, characterised

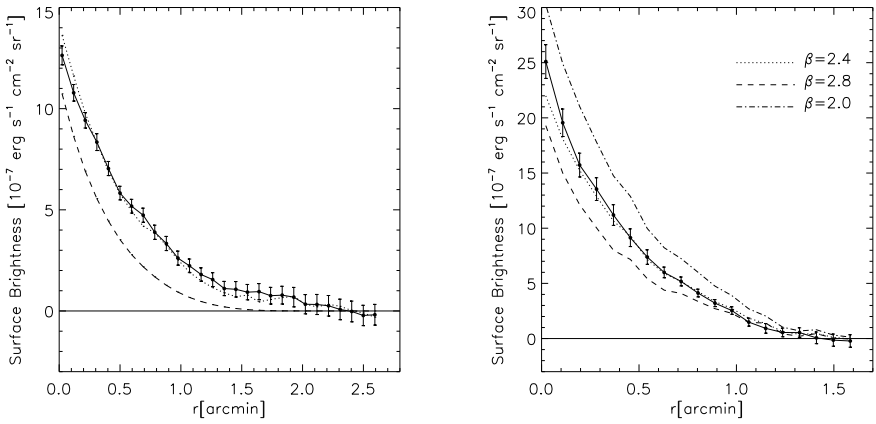

Figure 2.2: Left panel: The WFI halo profile with the contributions from the PSF (dotted line), and from the PSF with reduced wing amplitude (dashed). Right panel: The MOSCA halo profile and the best fit PSF contribution (dotted line). The other lines show the 1σ uncertainty of the fit. The values of β correspond to the index of the various power-laws we used to fit the PSF.

by the same behaviour as that of C IV λ1548 line that Sollerman et al. (2000) detected. The situation was not better with the Ca II λ3968 line. The feature that could indicate a blueshifted component out to -1700 km s^{-1} attributed to a halo is probably due to the red component of the Ca II λ3934 line, since no similar component has been seen in the blue part of the Ca II λ3934 line. The red part of the Ca II λ3968 line is mixed with the emission line of [Ne III] λ3967.5, thus we could not extract its profile.

2.2 Discussion

Based on the current measurements of Crab (i.e., mass, kinetic energy of the ejecta), and also on explosion models (Kitaura et al. 2006) for stars like the progenitor of the Crab, it is evident that there are problems with the mass and the kinetic energy. Models from Kitaura et al. (2006) suggest that the ejcta from explosions of stars in the mass range $8-9$ M$_\odot$ will have a kinetic energy between $0.6-1.5 \times 10^{50}$ ergs. This amount of energy is higher than the measured kinetic energy in the Crab by a factor of $2-5$. Thus an amount of mass should be present in the form of an undetected halo. In terms of its radial density profile, $\rho \propto \mathrm{R}^{-\eta}$ is assumed, and a reasonable temperature is 2×10^4 K. Profiles with index $\eta < 3$, are not able to fit the UV results from Sollerman et al. (2000), while those with $\eta \geq 5$, are not favoured, since this would make the Hα brightness surpass our detection limit.

Both our photometric and spectroscopic observations searching for a faint halo around the Crab were not fruitful. Problems with PSF contamination in photometry and low S/N ratio in spectroscopy were the reasons for the negative results. From the experience we had with photometry, a possible repetition of the halo search will require some initial thoughts. Starting with sky conditions, the observations must be carried out around the new moon, to keep the sky background as low as possible. The other important issue is PSF contamination. In Paper I, we showed the effect of the PSF in detail, so in any future attempt, good knowledge of the PSF of the instrument that will be used is essential. To make a "complete" data set, apart from the observations of the Crab nebula, time should be dedicated to taking images of bright and isolated stars to construct an accurate model of the PSF. The chosen star should be placed at the centre of the detector to create a PSF model that extends out to $2-3$ arcminutes. Choosing also an instrument with a uniform PSF across the chip is important, to make sure that we have a good feeling of the behaviour of the PSF wings across the CCD chip. A two dimensional convolution of the PSF model with the target image and with the hypothetical halo removed, can reveal if a halo is present or not.

The spectroscopic findings do not show evidence of any fast moving gas (i.e., $\geq$ 2500 km s^{-1}). The findings are in agreement with the results of Charlebois et al. (2010) where the highest velocities are found north of the pulsar. The fact that no similar profiles to that of Sollerman et al. (2000) were found in the Ca II absorption lines, could be related to the poor S/N ratio (the exposure time of the ALFOSC spectrum was only one hour), and also in the mixing with the emission lines that are nearby. There is also the issue of the low degree of ionisation of Ca II, which would make its column density too low to detect. Based on the data analysis it seems that searching for fast moving [O III] components would require massive amounts of telescope time. What is perhaps worthy to try is to search for fast Hα gas, since its emission can be boosted also by collisional excitation of Lyβ, followed by part of the radiative de-excitation going into Hα. This works only for temperatures above 10^4 K, which based on the halo models from Lundqvist et al. (1986) is a possible scenario (see Paper I for further details). An important outcome of Paper IV was that any spectroscopic search for fast line emission must be done at medium resolution (i.e., $\leq$ 150 km s^{-1}) as it would otherwise be impossible to disentangle the halo emission from emission from the fastest gas of the Crab nebula. Hα is blended with [N II] so a spectroscopic study of fast Hα must take that into account properly.

Part III:
A look at the heart of the Crab nebula

3. A look at the heart of the Crab nebula

In Paper II we focused on the Crab pulsar and its pulsar wind nebula (PWN), checking for temporal variations on its dynamic structure and emissivity, together with the spectral index across the PWN. My contribution to Paper II was the data reduction and interpretation of the results. A brief presentation of our optical and infrared data from Paper II is discussed below.

3.1 Results and Analysis

The task of the project was to investigate the emission mechanism of pulsars and their environments. For this purpose we chose to observe the Crab PWN. For the needs of the project we used both optical and infrared data. Optical data were collected using broad band optical filters (U, V, I) choosing filters that do not contain strong emission lines (e.g., Hα, [N II], [O III] etc), securing only continuum measurements. In the case of the IR data, we had two separate epochs using H and K_s filters with a time window of 75 days. The purpose of this time window was to check variation in the dynamic structure and emissivity of the Crab PWN. The results were compared with theoretical models (Spitkovsky & Arons 2005; Del Zanna et al. 2006), to cross-check the emission mechanism that is responsible for the observed features.

3.1.1 The Knot

Perhaps the most striking result with regard to the results of Hester et al. (1995) was the study of the knot near the Crab pulsar. This knot located at a distance of $0.''65$ has been reported to vary (Hester et al. 2002) in terms of emission and to remain stationary (Sollerman 2003). To make flux measurements of the knot in the optical and in the IR, we had to remove the pulsar from images. This was done by removing the pulsar from every image with the point spread function (PSF) (see Fig. 3.1). Thus in the case of the K_s band the flux of the knot is $\sim 10\%$ of the flux of the pulsar. For the H band the flux of the knot is $\sim 8\%$ of the pulsar's flux, while in the I band it is $\sim 6.5\%$ (see Table 3.1 for more details). Comparing the fluxes from the two IR epochs it

seems that there is no variation in the emission of the knot. The disagreement of the IR knot variation with the X-ray results of Hester et al. (2002), will be discussed below. Also from the data of the 13 December 2007, we estimated the spectral index of the knot to be $\alpha_\nu = -0.63 \pm 0.02$.

The high resolution of NOTCam allowed us to measure the distance between the knot and the Crab pulsar. This enabled us to check if the knot displays any proper motion with respect to the pulsar. To do this we compared our data with HST/WFPC2 data from 1994. We know that the pulsar has a proper motion of $0\farcs016$ yr^{-1} (Kaplan et al. 2008), so in the 13.5 years period between the two images a proper motion of $\sim 0\farcs2$ is expected. By using stars near the pulsar we found that foreground/background have shifted by this amount ($\sim 0\farcs2$), while the distance between the knot and the pulsar was the same ($\sim 0\farcs65$). From the pointing uncertainties of IRAF's PHOT, we set an upper limit for knot velocity relative to the pulsar. Based on the fact that the knot lies along the jet axis and that the jet axis is tilted $\sim 30^\circ$ to the plane of the sky (Hester 2008) as well as taking into account that the pulsar also moves along the jet axis, the knot trails the pulsar by ≤ 10 km s^{-1}, corresponding to $\leq 6\%$ of the space motion of the pulsar. But since the pointing uncertainties were the same for the background/foreground stars too, it is safe to state that the knot is associated with the pulsar, thus both moving together in terms of proper motion.

3.1.2 The wisps

The arc-like structures that are seen in the Crab PWN along the jet axis are referred to as wisps. Using optical and IR data, our task was to check their dynamical and emissivity variation and measure their spectral indices. As can be seen in Fig. 3.1, two wisps in the eastern south-eastern direction of the pulsar can be distinguished, while on the other direction of the jet a triplet is present. From the IR data we found a variation of 20% on average. Unlike the knot, the wisps display outward shifts. For the brightest wisp (wisp 2), the outward shift corresponds to a velocity of ~ 0.22c. Finally, in the H-band image of December 13, we see that the pulsar is surrounded by a dim halo which has also been seen in the X-rays by Chandra. A complete picture of the photometric measurements of the wisps and the knot is given in Table 3.1.

Using the U $\rightarrow$ K_s data, we made estimates on the spectral index across the PWN. The regions are located across the jet axis (see Fig. 3.1), while for dereddening the fluxes we used $R_V = 3.1$ and $E(B-V) = 0.52$ mag. The spectral indices for each wisp and interwisp region (i.e., the area between the wisps) were estimated by fitting a linear function. All the results show that the wisps and the interwisps regions display red spectra with similar spectral indices (α_ν =-0.63 $-$ -0.49), suggesting that synchrotron emission is the mechanism responsible for powering the Crab PWN.

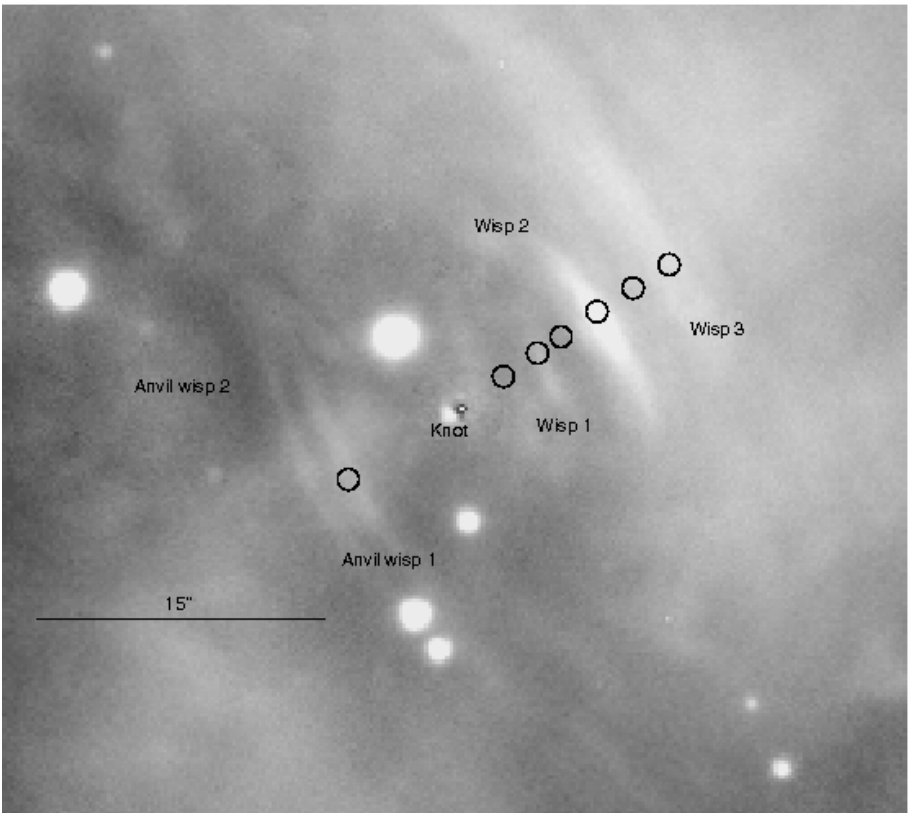

Figure 3.1: I-band image of the Crab nebula taken with ALFOSC at the NOT on 7 December 2007. The pulsar has been removed with PSF subtraction to reveal the nearby knot that lies at a distance of $0\farcs65$. The field of view is $\sim 45\times45$ arcseconds, with north pointing upwards and east to the left. The areas that we used to measure the emission from the wisps and the interwisp regions are marked with circles.

3.1.3 The Crab vs. other PWNe

Studies of other PWNe (e.g., Vela, Crab, 3C58) have shown similar spectral energy distributions, suggesting a similar emission mechanism for these PWN. Using Chandra data, Pavlov et al. (2001), found that Vela displays a slightly flatter spectra in its PWN than the Crab (i.e., α_ν ranges from -0.5 to -0.3). Just like the Crab PWN, variations in the Vela PWN have been reported of up to 30 % (Pavlov et al. 2001). The PWN of Vela has not yet been detected in optical wavebands, but Shibanov et al. (2003), using IR data managed to detect structures around the pulsar that overlap with those in X-rays, suggesting a very steep red spectrum. Another interesting pulsar that is usually referred to as the Crab twin is PSR B0540-63.9 in the LMC. Using HST data from U to I, Serafimovich et al. (2004) measured the spectral index across the PWN of PSR B0540-63.9. On average the spectral index was found to vary across the remnant from -1.58 to -0.27. Another interesting and well studied PWN is

Table 3.1: Photometric results [a] for the Crab wisps and the knot

Filter	Int. Wisp 1	Wisp 1	Wisp 2	Wisp 3	Anvil Wisp 1	Knot
U	1.70(0.10)[b] [c]	1.70(0.10)[d]	2.35(0.10)	2.05(0.10)	1.45(0.10)	-[e]
V	1.70(0.10)	1.80(0.10)	2.65(0.10)	2.30(0.10)	1.65(0.10)	-
I	1.75(0.10)	1.95(0.10)	2.85(0.10)	2.40(0.10)	1.75(0.15)	1.60(0.10)
H	3.25(0.15)	3.95(0.15)	6.25(0.25)	4.75(0.20)	3.60(0.15)	2.75(0.10)
K_s	4.05(0.15)	4.45(0.15)	6.45(0.25)	4.90(0.20)	4.10(0.15)	2.90(0.10)

[a] The IR results are from the night of 13 December 2007.
[b] Flux in units of ergs s^{-1} cm^{-2} Hz^{-1} $\times 10^{-27}$. Brackets give the 1-σ uncertainty.
[c] The first interwisp region lies between the pulsar and wisp 1, the second between wisps 1 and 2 and the third lies between wisps 2 and 3.
[d] We used $E(B-V) = 0.52$ mag and $R_V = 3.1$ for derreddening.
[e] No measurements were made.

3C58. Using data from radio to IR, Shibanov et al. (2008) estimated a spectral index in the range -1.2 to -0.5 depending on the extinction correction that is used. The similarity of the spectral energy distribution these PWN display, is striking. Further detailed observations should be made to see how the spectral indices vary with distance from the pulsar throughout the electromagnetic spectrum, to understand the cooling of the electrons.

3.2 A view on the Crab PWN

The IR data (presented in Paper II) suggest changes in the inner environment of the Crab for both dynamic structures and emissivity. The estimated velocities for the shift of the wisps seem to agree with Tanvir et al. (1997), but not with those of Hester et al. (2002), where velocities of up to ~ 0.5c have been claimed. This could be due to the large time window we had between the two IR datasets (75 days), since Hester et al. (2002), measured similar shifts for optical and X-ray wavebands. Regarding the inner knot, our results are in agreement with the results from Melatos et al. (2005), while Sandberg & Sollerman (2009) reported a steeper spectral index for the knot of $\alpha_\nu = -1.3$, using UBRIz data. For the IR-part alone, however, they get a flatter profile. The disagreement between our findings and those of Sandberg & Sollerman (2009), suggests that further observations are needed in the form of a daily monitoring program to check the diversity in the value of the spectral index of the knot.

Variations in the emissivity on a long time scale can be explained by instabilities in the emission mechanism of the pulsar (Hester et al. 1995; Del Zanna 2006). By comparing our results with theoretical models, we found that the synthetic spectra of Del Zanna et. al (2006) agree with our observations. The short time scale variations (i.e., kilosecond time scale) are still not

well understood. Melatos et al. (2005) measured variations in the NIR of up to 24% in the J band, so it would be useful to check this in optical wavebands too, and also variation in the spectral energy distribution as well.

Because there are many open questions regarding the nature of PWNe in general, it would be interesting to extend this project to other Crab-like remnants to identify similar structures. In Paper II we made some observational comparisons with other PWNe, but a more detailed comparison in terms of structure, temporal behavior, and polarization properties is needed.

Part IV:
The outer rings of SN 1987A

4. The outer rings of SN 1987A

The triple ring system of SN 1987A has offered a unique opportunity to study the properties and evolution of circumstellar matter around massive stars. Since their discovery, the rings have been studied extensively, especially the inner ring (or equatorial, ER as we have defined it before). In a recent article, Mattila et al. (2010) discussed the evolution of the ER. Based on this we decided to monitor the evolution of the outer rings (ORs), trying to understand the nature of the ring system. In Paper III we used archive photometric HST data from the WFPC2 and ACS, and spectra from FORS1 and UVES on VLT. My contribution was the data reduction and analysis of the FORS1 data, and also on the analysis of the photometric data. Per Gröningsson worked with the UVES data, while my supervisor Peter Lundqvist worked on the interpretation of the plasma diagnostics of the ORs, and the models we used for it. Finally, Soroush Nasoudi Shoar provided contribution to the initial stages of the analysis of the photometric data.

4.1 Results and analysis

4.1.1 Spectroscopy

For both the FORS1 and UVES data we measured the Balmer line fluxes, and extracted important information using plasma diagnostics for various forbidden lines (e.g., [N II], [O III], [S II]). For the Balmer lines, our findings are close to what Case B predicts, (see Osterbrock & Ferland 2006) with the exception of the $j_{H\alpha}/j_{H\beta}$, a difference that can be attributed to collisional excitation of Hα (Lundqvist & Fransson 1996). The other two cases with ratios higher than what Case B predicts ($j_{H\varepsilon}/j_{H\beta}$ & $j_{H\zeta}/j_{H\beta}$), are due to the fact that FORS1 has a poor resolution and we were not able to distinguish the Balmer lines from [Ne III] λ3967.5 and He I λ3888.7, respectively.

From the line ratios of forbidden lines we could estimate the density and temperature of the ORs. The fact that two spectroscopic epochs were available allowed us to monitor the evolution of both rings. Thus in the 2002 epoch, for the SOR, an estimated electron temperature of $1.95-2.00\times10^4$ K for the [O III] gas was found, while for the [N II] gas it was $1.0-1.1\times10^4$ K. Assuming that the temperature of the [S II] gas is not higher than in the [N II] gas, an electron density of $N_{\rm e}\sim 3.3\times10^3$ cm^{-3} was estimated. Also, by using the [O III] temperature as a maximum, an electron density of $N_{\rm e}\sim 1.0\times10^3$ cm^{-3},

was estimated for the [O II] gas. For the 2009 epoch, the temperature of the [O III] gas seems to be the same as in 2002, which was also the case for [N II]. The estimated gas densities are $N_e \sim 3.0 \times 10^3$ cm^{-3} and $N_e \sim 2.3 \times 10^3$ cm^{-3} for [S II] and [O II] respectively. For the 2002 epoch, and the NOR, we got an [O III] temperature of $\sim 2.7 \times 10^4$ K, and an [N II] temperature of $\sim 1.2 \times 10^4$ K. For the electron density, the result of the NOR is consistent with that of the SOR, but the [O II] density was not possible to measure. For the 2009 epoch the derived value for [N II] was still $\sim 1.2 \times 10^4$ K.

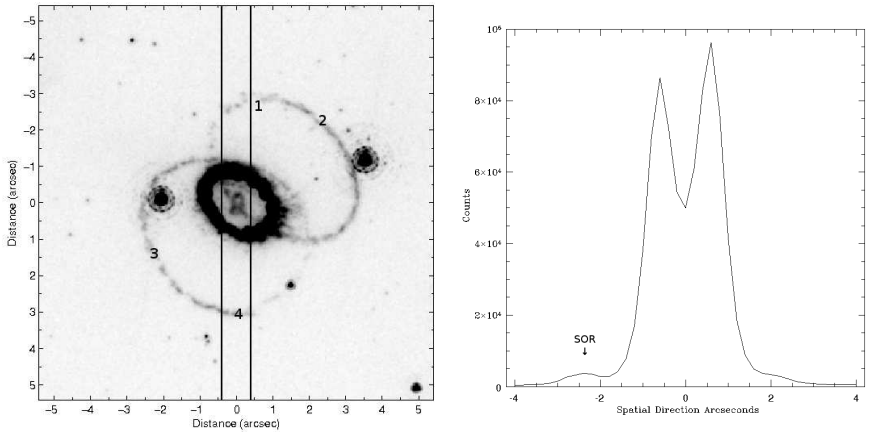

Figure 4.1: Left panel: HST/ACS image (filter F658N) of the triple ring system of SN 1987A from January 2003 (obtained by the SAINTS team; PI: R.P. Kirshner). The slit position of the VLT/UVES observations is superposed (the slit width is $0\farcs8$ and PA=30°). The numbers (1−4) correspond to the locations for which we did the photometric measurements. Right panel: Flux of [N II] λ6583 across the slit. The southern outer ring can be seen on the left side of the figure at $2\farcs4$ from the centre of the remnant.

4.1.2 Photometry

We used photometry to obtain lightcurves for the [O III], [N II] and Hα emission. In paper III details on the photometric analysis are described, together with the lightcurves (see Fig. 10 in the paper). The high uncertainties in the [O III] measurements did not allow us to make estimates of the evolution of the [O III]/Hα ratio. Estimates were nonetheless made for the [N II] emitting gas. Thus for SOR, the [N II]/Hα ratio for the 1994 was estimated to be $\sim$ 2.00. For the 1996 this increased to $\sim$ 2.10, while from the UVES data (2002 epoch) a line ratio of $\sim$ 2.25 was estimated. In the same manner for NOR, for the 1994 epoch we estimated a ratio of $\sim$ 2.05. For the 1996 epoch this increased to $\sim$ 2.13, and moved up to $\sim$ 2.27 for the 2001 epoch and further to $\sim$ 2.37 for the 2003 epoch. Due to the lack of WFPC2 data for 2004 and 2005, no estimates of the [N II]/Hα line ratio were made.

The lightcurves of the Hα and the [N II] lines decay as expected for cooling and recombining gas. The [O III] lightcurve has a different appearance at late times which could be due to contamination or possibly re-ionisation. To make estimates of the decay time of the lightcurves, we made fits to the line lightcurves with the function $f_{\rm line} = Cexp(-t_{\rm corr}/t_{\rm efold})$, where $t_{\rm corr}$ is the corrected delay time (see Paper III for details Sect. 4.1), and $t_{\rm efold}$ is the decay time of the line flux. For Hα, the decay times are $\sim 2.8 \times 10^3$ days and $\sim 4.2 \times 10^3$ days for Areas 4 and 1, respectively. For [N II], we obtained $\sim 3.2 \times 10^3$ days and $\sim 4.6 \times 10^3$ days for Areas 4 and 1, respectively, and for [O III] $\sim 2.9 \times 10^3$ days and $\sim 6.8 \times 10^3$ days, respectively. In general, the fluxes fall faster in SOR (Area 4) than in NOR (Area 1). The long decay time for [O III] in Area 1 should be regarded with caution, as the [O III] ACS data from 2003 & 2004 are uncertain.

4.2 Diagnostics from the outer rings

The plasma diagnostics from spectroscopy suggest that the ORs are similar between them in terms of physical conditions (i.e., density & temperature). The emission from both ORs is due to recombination and cooling, just like in the ER (Lundqvist & Fransson 1996, Mattila et al. 2010). From preliminary modeling of the photometry (Lundqvist 2007), we know that the ORs are rich in nitrogen (i.e. CNO processed material). This matter may have been dredged up to the stellar surface by convective mixing. This also suggests that the progenitor of SN 1987A went through a RSG phase prior to its BSG phase before the explosion. This also agrees with the current theoretical models for the progenitor of SN 1987A (Morris & Podsiadlowski 2007).

To explain the lightcurve profile of Hα, apart from recombination, we need to invoke collisional excitation too. For this to happen a temperature of $\geq$ (1.0 - 1.5) $\times$ 10^4 K is needed. This seems to be valid, since we estimated a temperature close to that from spectroscopy. Hα is also useful since its long photometric decay gives us an estimate of the highest densities in the ORs. To model the slow decline of the other lines we need to invoke a distribution of densities just like for the ER (Mattila et al. 2010). In particular [N II] is useful for estimating the relative distribution of the different mass components.

A star that is similar to SN 1987A is Sher 25 (Brandner et al. 1997). Just like SN 1987A, high CNO ratios have been derived (Brandner et al. 1997), suggesting that the star also went through a RSG phase prior to its current BSG phase. What is interesting with Sher 25 is that the two outer lobes are denser than its inner ring (Brandner et al. 1997), being the opposite case to the rings of SN 1987A.

In Paper III the future of SN 1987A was also discussed, especially the collision of the supernova ejecta with the ORs. The collision of the ER is now active and has made it to the front page of journals. Unlike the ER, the

collision of the ORs will be more moderate. The future of SN 1987A will therefore continue to provide a testbed for new telescopes and instruments. Telescopes like ALMA and JWST, and their successors, will reveal the true structure of the circumstellar gas of SN 1987A. Our density estimates, as well as estimates for the orientation of the ORs, will hopefully prove useful when interpreting such future data.

Part V:
Summary

5. Summary

Through these three projects, some questions were answered, some remained unanswered, while some were raised. In the project were I tried to detect a halo around the Crab, despite the fact that no halo was found, more efficient observing techniques were suggested for projects that deal with low surface brightness measurements in general (e.g., shells around SNRs or galactic haloes). A deeper photometric search, or spectroscopy with HST in the UV and large ground-based telescopes in the optical are essential to cast more light to the so far enigmatic nature of the Crab nebula. Even if no halo will be detected, this can perhaps be used as evidence to call for a revision of the explosion models of stars in this mass range (9-10 $M_{\odot}$).

The program for the pulsar the Crab pulsar, in my view, acted as an introduction to future observations of other PWNe too. The observations of the Crab confirmed that models for the plasma motions while through proper motion tests, it was found that the nearby knot is stationary with respect to the pulsar. In terms of the dynamical variation in the Crab, observations with a time window of a week will be more efficient to check if the X-ray shift of the wisps (0.5c), coincides with the one in the optical and infrared. The spectral index of the Crab is more or less similar to the spectral indices of other PWN (i.e. Vela, 3C 58), but what would be more interesting to do, would be a program where pulsars of different age and morphology are compared in terms of dynamic and emissivity variation.

The monitoring program of the outer rings of SN 1987A showed that the two rings are not different in composition, or in terms of their physical conditions. Recombination and cooling, seem to be responsible for the evolution of the emission lines just like in the inner ring (Lunqvist & Fransson 1996), the initial heating being provided by the UV flash from the explosion. SN 1987A has cast a lot of light on core collapse supernova research, since it confirmed the core collapse models (e.g., from the neutrino detection), and also let us discover that even a blue supergiant can explode as a supernova. Finally, the ring system offered a unique opportunity, to study the interaction of CSM with the supernova ejecta, and through comparison with objects like Sher 25 understand the mass loss mechanism in massive stars. Both SN 1987A and the Crab will undoubtedly continue to serve as benchmarks for supernova research and the evolution of massive stars for a long time to come.

Part VI: Acknowledgements

This is the part which most people read, so it will be short. First of all, I would like to thank my supervisor Peter Lundqvist for his guidance, on my research projects all these years. Also thanks to Jesper Sollerman, for providing useful comments during data analysis. I am more than grateful to Michael Schirmer, for helping me with the analysis of the WFI data, and providing a pipeline that proved to be really useful in treating data sets of this size and kind. Göran Olofsson provided crucial comments on my first article and showed me methods in data analysis that turned out to be more than useful. So I am really glad he did, even though that meant that interpretations of my results were not those desired.

Also the staff of the Department that spent time teaching the courses of the PhD program, Roland Svensson for the Gas dynamics course, Göran Scharmer & Mats Löfdahl for the Stellar atmospheres course, Pawel Artymowicz for the galaxies course, Rene Liseau for the Observational techniques course, Göran Östlin for the galaxies course, Peter Lundqvist for the ISM course, Claes Fransson for the high energy course, Fredrik Larsen Schöier for the radiation processes course, and Garrelt Mellema for the Stellar evolution course. Apart from the staff that teaches the courses I would like to thank Robert Cumming for answering my questions. Additionally, I would like to thank the people that take care of administrative work in the Department, Lena Olofsson, Sandra Åberg, and Ulla af Petersens. Also I would like to thank many of the students for the useful, or not so useful conversations we had. I would like to thank Matthew Hayes, and Andreas Lundgren for maintaining a warm environment in the office, during the time we spent together, also Torsten Elfhag for answering my aviation questions. Also I would like to thank Miguel de Val Borro for sharing the same ideas with me on football. Jacob Trier Frederiksen, Jens Melinder, Jaime de la Cruz Rodriguez, and the rest of the PhD students for the interesting nights

out in Stockholm. Last but not least Uno W*ä*nn and Alexis Brandeker for the conversations we had in my mother tongue.

Apart from the people in Stockholm I would also like to thank the staff at the Nordic Optical Telescope in La Palma for making my stay there really pleasant. First of all I would like to thank Johannes Andersen and Thomas Augusteijn for giving me the opportunity to work for a year at the telescope site. During that year I managed to learn a lot on observing techniques and data analysis. I would like to thank the technicians and the IT team there for providing support, and thus making the telescope operational. These are, Peter Brandt, Ricardo Cardenes, Jacob Clasen, Graham Cox, Carlos Perez, and Peter Sorensen. I would like to thank Tapio Pursimo and John Telting for providing hints on data analysis, and Anlaug Amanda Djupvik for introducing me to IR astronomy. Last but not least I would like to thank Ingvar Sv*ä*rdh for making sure that the telescope is fully and safely operating, and also Paco Armas and Loida Fernandez for the help they provided with the paper work when I first moved there. I shouldn't also forget to thank Jarkko Niemel*ä* and Carolin Villforth for the good times I had there.

Part VII:
Bibliography

6. Bibliography

Arnett, D., 1989, ApJ, 343, 834
Aschenbach, B., & Brinkmann, W. 1975, A&A, 41, 147
Baade, W. & Zwicky, F. 1934, Proceedings of the National Academy of Sciences of the USA, Vol. 20, Iss, 5, p. 254
Bietenholz, M. F. & Kronberg, P. P., 1992, ApJ, 393, 206
Bildsten, L., Chakrabarty, D., Chiu, J., et al. 1997, ApJS, 113, 367
Blair W. P., Long K. S., Vancura O., et al. 1992, ApJ, 399, 611
Blinnikov, S., Lundqvist, P., Bartunov, O., et al., 2000, ApJ, 532, 1132
Blondin, J. M. & Lundqvist, P. 1993, ApJ, 405, 337
Blondin, J. M., Mezzacappa, A., & DeMarino, C. 2003, ApJ, 584, 971
Brandner, W., Chu, Y.-H., Eisenhauer, F., et al. 1997, ApJ, 489, L153
Burrows, C. J., Krist, J., Hester, J. J. et al. 1995, ApJ, 452, 680
Charlebois, M., Drissen, L., Bernier, A. P. et al. 2010, AJ, 139, 2083
Chen W., & Gehrels, N., 1999, ApJ 514, L10
Chevalier, R. A. 1977, in Supernovae, ed, D. Schramm
Chevalier, R., A. 1985, in The Crab Nebula and related supernova remnants, Cambridge Univ. Press., p. 73
Chevalier, R. A., 2005, ApJ, 619, 839
Chugai, N. N., Blinnikov, S. I., Cumming, R. J., et al. 2004, MNRAS, 394, 21
Cioffi, D.F., 1990, in Physical processes in hot cosmic plasmas, ARI, p. 1
Clark, D. H., Murdin, P., Wood, R. et al. 1983, MNRAS, 415, 431
Cocke W. J., Disney M. J., Taylor D. J. 1969. Nature, 221, 525
Comella, J. M., Craft, H. D., Lovelace, R. V. E., & Sutton, J. M. 1969, Nature, 221, 453
Crotts, A. P. S., Kunkel, W. E., & McCarthy, P. J. 1989, ApJ, 347, 61
Crotts, A. P. S., & Heathcote, S. R. 2000, ApJ, 528, 426
Crotts, A. P. S. 2007, in Supernova 1987A: 20 Years After: Supernovae and Gamma-Ray Bursters., Vol. 937 (AIP Conference Proceedings), p. 112
Dessart, L., Hillier, D. J., Gezari, S., et al. 2009, MNRAS, 394, 21
Del Zanna, L., Amato, E., & Bucciantini, N., 2004, A&A, 421, 1063
Del Zanna, L., Volpi, D., Amato, E., & Bucciantini, N., 2006, A&A, 453, 621
Fesen R. A., Kirshner R. P., 1982. ApJ., 258, 1
Fesen, R., A., Shull, J., M., Hurford, A., P., 1997, AJ, 113, 354
Fesen, R. A., Hammell, M. C., Morse, J., et al., 2006, ApJ, 645, 283

Filippenko, A. 1997, ARA&A 35, 309
Fransson, C., Lundqvist, P. 1989, ApJ, 341L, 59
Gaensler, Bryan M., & Slane, Patrick O., 2006, ARA&A, 44, 17
Garnavich, P. M., Kirshner, R. P., Challis, P., et al. 1999, AAS, 195, 4303
Gibson, K., Stetson, P. B., Freedman, W. I., et al. 2000, ApJ, 529, 723
Gold, T. 1968, Nature, 218, 731
Gröningsson, P., Fransson, C., Leibundgut, B. et al. 2008 A&A, 492, 481
Graham J. R., Wright G. S., Longmore A. J. 1990. ApJ, 352, 172
Graves, G. J. M., Challis, P. M., Chevalier, R. A., et al. 2005, ApJ, 629, 944
Gull T. R., Fesen R. A. 1982. ApJ, 260, L75
Heger, A., Fryer, C. L.,Woosley, et al. 2003, ApJ, 591, 288
Hester, J. J., Scowen, P. A.; Sankrit, R., et al. 1995, ApJ, 448, 240
Hester, J. J., Stone, J. M., Scowen, et al. 1996, ApJ, 456, 225
Hester, J. J., Mori, K., Burrows, D., 2002, ApJ, 577L, 49
Hester, J. J., 2008, ARA&A 46, 127
Janka, H. T., Marek, A., Müller, B., & Scheck, L. 2008, in 40 Years of pulsars: Millisecond Pulsars, Magnetars and More., Vol. 983 (AIP Conference Proceedings), p. 369
Kargaltsev, O., Pavlov, G. G., in 40 Years of pulsars: Millisecond Pulsars, Magnetars and More. AIP Conference Proceedings, 983, 171
Kitaura, F. S., Janka, H.-Th., Hillebrandt, W. 2006, A&A, 450, 345
Kiziltan, B., Kottas, A., & Thorsett, S. E., 2010, arXiv:1011.4291
Krause, O. Birkmann, S. M., Usuda, T., et al. 2008, Sci, 320, 1195
Langer, N. 1991, A&A, 243, 155
Lampland, C. O. 1921, PASP, 33, 79
Leibundgut, B., 2000, ARA&A, 10, 179
Lundqvist, N., Lundqvist, P., Björnsson, C.-I., et al. 2011, MNRAS, tmp, 105L
Lundqvist, P., Fransson, C., & Chevalier, R. A. 1986, A&A, 162L, 6
Lundqvist, P., & Fransson, C., 1996, ApJ, 464, 924
Lundqvist, P., 1999, ApJ, 511, 389
Lundqvist, P. 2007, in Supernova 1987A: 20 Years After: Supernovae and Gamma-Ray Bursters., Vol. 937 (AIP Conference Proceedings), p.102
Lundqvist, P., & Tziamtzis, A., 2011, in prep.
MacFadyen A. I., Woosley S. E., & Heger A. 2000, ApJ, 550, 410
Maran, S. P., Sonneborn, G ., Pun, C. S. J., et al, 2000, ApJ, 2000, 545, 390
Martin, C. L. & Arnett, D. 1995, ApJ, 447, 378
Matheson, H., & Safi-Harb, S., 2005, AdSpR, 35, 1099
Mattila, S., Lundqvist, P., Gröningsson, P., et al. 2010, 717, 1140
Melatos, A., Scheltus, D., Whiting, M. T., et al. 2005, ApJ, 633, 931
Meyer, F. 1997, MNRAS, 285, L11
Meyer, F. 1999, Highlights in x-ray astronomy, 1999, MPE report, 272, p.324

Meynet, G. & Maeder, A. 2005, A&A, 429, 581
Minkowski, R. 1941, PASP, 53, 224
Mori K, Burrows D. N, Hester J. J, et al. 2004, ApJ, 609, 186
Morris, T. & Podsiadlowski, P. 2007, Science, 315, 1103
Nomoto, K. 1985, in The Crab Nebula and related supernova remnants, Cambridge Univ. Press. p. 97
Kaplan, D. L., Chatterjee, S., Gaensler, B. M., & Anderson, J. 2008, ApJ, 677, 1201
Komissarov, S. S., & Lyutikov, M., 2010, astro-ph:0911.0608
Oort, J. H. & Walraven, Th. 1956, BAN, 12, 285
Oppenheimer, J. R. & Snyder, H., 1939, Phys. Rev., 56, 455
Oppenheimer, J. R., & Volkoff, G. M. 1939, Phys. Rev., 55, 374
Osterbrock, D. E., & Ferland, G. J. 2006, Astrophysics of gaseous nebulae and active galactic nuclei. Univ. Sci. Books.
Panagia, N., Scuderi, S., Gilmozzi, R. et al. 1996, ApJ, 459L, 17
Panagia, N. 1999, in New Views of the Magellanic Clouds, IAU Symposium 190, 549
Pavlov, G. G., Sanwal, D., Garmire, G. P., & Zavlin, V. E., 2001, Neutron Stars in Supernova Remnants, ASP Conference Series, Vol. 271, p.247
Perlmutter, S., Gabi, S., Goldhaber, G., 1997, ApJ, 483, 565
Plait, P. C., Lundqvist, P., Chevalier, R. A., & Kirshner, R. P. 1995, ApJ, 439, 730
Preibisch, T., & Zinnecker, H., 2001, in From Darkness to Light: Origin and Evolution of Young Stellar Clusters. Astron. Soc. of the Pacific, p. 791.
Podsiadlowksi, P. 1992, PASP, 104, 717
Romani R. W., Reach W. T., Koo B. C., Heiles C. 1990, ApJ, 349, L51
Sandberg, A., & Sollerman, J. 2009, A&A, 504, 525
Sankrit R., Hester J. J., 1997. ApJ, 491, 796
Sankrit, R., Hester, J. J., Scowen, P. A., et al., 1998, ApJ, 504, 344
Scargle, J. D. 1969, ApJ, 156, 401
Schawinski, K., Justham S., Wolf C., et al., 2008, Science, 321, 223
Shaposhnikov, N., & Titarchuk, L. 2007, ApJ, 663, 445
Shibanov, Y. A., Koptsevich, A. B., Sollerman, J., & Lundqvist, P., 2003, A&A, 406, 645
Shibanov, Y. A., Lundqvist, N., Lundqvist, P., et al., 2008, A&A, 486, 273
Sedov, I. I., 1959, Similarity and dimensional methods in mechanics, Academic Press, New York
Serafimovich, N. I., Shibanov, Y. A., Lundqvist, P., & Sollerman, J., 2004, A&A, 425, 1041
Sollerman, J., Lundqvist, P., Lindler, D., et al. 2000, ApJ, 366, 197
Sollerman, J., Kozma, C., Lundqvist, P., 2001, A&A, 366, 197
Sollerman, J. 2003, A&A, 406, 639
Spitkovsky A, & Arons J. 2004, ApJ, 603, 669

Staelin, D., H., & Reifenstein, E., C., III, 1968, Science, 168, 1481
Sugerman, B. E. K., Lawrence, S. S., Crotts, A. P. S., et al. 2002, ApJ, 572, 209
Sugerman, B. E. K., Crotts, A. P. S., Kunkel, W. E., et al. 2005, ApJ, 627, 888
Suntzeff, N. B., Phillips, M. M., Covarubias, R., et al. 1999, AJ, 117, 1175
Tanvir, N. R., Thomson, R. C., & Tsikarishvili, E. G. 1997, New Astronomy, vol. 1, no. 4, p. 311
Trimble, V., 1985, in The Crab Nebula and related supernova remnants. Cambridge Univ. Press, p. 257.
Truran, J.W. & Weiss, A. 1987, in Nuclear astrophysics; Proceedings of the Workshop, p. 293
Turatto, M., 2003, Supernovae and Gamma-Ray Bursters. Lecture Notes in Physics, vol. 598, p.21
Tziamtzis, A., Schirmer, M., Lundqvist, P., & Sollerman, J. 2009, A&A, 497, 167
Tziamtzis, A., Lundqvist, P., Gröningsson, P., & Nasoudi-Shoar, S., 2010, A&A, 572,35
Van der Swaluw, E., Achterberg, A., Gallant, Y. A., & Toth, G. 2001, A&A, 380, 309
Walborn, N. R., Prevot, M. L., Prevot, L., et al. 1989, A&A, 219, 229
Wallace, B. J., Landecker, T. L., Kalberla, P. M. W., & Taylor, A. R. 1999, ApJS, 124, 181
Wampler, J., Schwarz, H. E., Andersen, J., & Beresford, A. C. 1988, IAUC, 4541, 2
Wampler, E. J., Wang, L., Baade, D., et al. 1990, ApJ, 362L, 13
Wamsteker, W., Panagia, N., Barylak, M., et al. 1987, A&A, 177L, 21
Washimi, H., Tanaka, T., Shibata, S., 1999, ASSL, 240, 347
Wheeler, J. C., & Harkness, R. P. 1968, American Scientist, 56, 1
Woosley, S. E. 1993, ApJ, 405, 273
Woosley,S. E., Heger, A., Weaver, T. A., 2002, RvMP, 74, 1015
Woosley, S. & Janka, T. 2005, Nature, 1, 147
Utrobin, V. P., 2005, Astronomy Letters, Vol. 31, Issue 12, p.806
Vink, J., 2004, Advances in Space Research, Vol. 33, Issue 4, p. 356
Zhekov, S. A., McCray, R., Borkowski, K., et al. 2006, ApJ, 645, 293